Chemistry–A European Journal
Review
doi.org/10.1002/chem.202403760
Chemistry Europe
European Chemical Societies Publishing
www.chemeurj.org

Metal-Organic Framework (MOF)-Based Sensors for Mercury (Hg) Detection: Design Strategies and Recent Progress

Wei Ma,[a, b, c] Qidu Zhang,[d] Dongshan Xiang,*[a, b] Kang Mao,*[c] Jiaqi Xue,[c] Zhuo Chen,[c] Zhen Chen,[c] Wei Du,[e] Kun Zhai,[a, b] and Hua Zhang[c]

Monitoring mercury (Hg) is critical for environmental and public health. Metal-organic framework (MOF)-based sensors demonstrate the advantage of high sensitivity and rapid response. We summarize the advances of MOF sensors for Hg^{2+} detection from the perspective of MOF type and role in the sensors. First, we introduce three MOFs used in Hg sensors-UIO, ZIF, and MIL-that have demonstrated superior performance. Then, we discuss the specifics of MOF-based sensors for Hg^{2+} detection in terms of the recognition and signal elements. Currently, the recognition elements include T-rich aptamers, noble metal nanoparticles, central metal ions, and organic functional groups inherent to MOFs. Sensors with fluorescence and colorimetric signals are the two main types of optical MOF sensors used for Hg detection. Electrochemical sensors have also been fabricated, but these are less frequently reported, potentially due to the limited conductivity and cycling stability of MOFs. Notably, dual-signal sensors mitigate background signals interference and enhance the accuracy of Hg^{2+} detection. Furthermore, to facilitate portability and user-friendliness, portable devices such as microfluidics, paper-based devices, and smartphones have been developed for Hg^{2+} detection, showcasing potential applications. We also address the challenges related to MOF-based sensors for Hg^{2+} and future outlook.

1. Introduction

Mercury (Hg) is a pollutant that poses a serious threat to the environment and to human health worldwide.[1] For example, Hg in Guizhou in China,[2] in the Bay of Trieste in Slovenia[3] and in Almaden in Spain[4] has reached levels of 22–360 ng/L, 2.8–322 ng/L and 7.6–20300 ng/L, respectively. The toxicity of various Hg compounds varies significantly, with methylmercury being considerably more toxic than other forms.[5] Unlike elemental and inorganic forms of Hg, methylmercury exhibits high lipid solubility, which enables it to accumulate in aqueous environments,[6] be absorbed by plants,[7] and be ingested by animals, by which route it can enter food chains[8] and ultimately affect human health, causing disorders such as nervous system defects, arrhythmia, cardiomyopathy, and kidney damage.[5c,9] Therefore, the development of efficient analytical methods for the detection of Hg in the environment and in food is crucial for identifying Hg contamination and for risk assessments.[10]

Traditional Hg^{2+} detection methods include mainly atomic emission spectrometry (AES),[11] atomic absorption spectrometry (AAS) [9],[12] and inductively coupled plasma mass spectrometry (ICP-MS),[13] which have high sensitivity, excellent stability, superior selectivity, broad detection ranges, and good automation capabilities.[14] However, these techniques have limitations, including labour-intensive testing procedures, complex sample preparation processes, costly equipment, and the need for skilled personnel.[15] Therefore, given the complexity of environmental matrices, the existence of numerous interference factors, time constraints, and the drawbacks associated with conventional detection methods, such as lengthy cycles and elevated costs, it is vital to advance research on the development of efficient and rapid on-site Hg^{2+} detection methods.

Sensors have emerged as novel technologies and have attracted widespread interest owing to their high precision, rapid response rates, miniaturization and integration capabilities, good reliability, and robust environmental adaptability.[16] These sensors identify target compounds using a recognition element, and the recognition process is transformed into a specific signal by a transduction element. This signal then enables the target compound to be detected qualitatively or quantitatively.[17] The recognition elements can be antibodies, enzymes, aptamers, or functional materials, all of which can be specifically recognized.[18] The signal elements include optical,

[a] W. Ma, D. Xiang, K. Zhai
School of Chemistry and Environmental Engineeing, Hubei Minzu University, Enshi, 445000 China
E-mail: zk3100@sohu.com
[b] W. Ma, D. Xiang, K. Zhai
Hubei Key Laboratory of Selenium Resource Research and Biological Application, Hubei Minzu University, Enshi, 445000, China
[c] W. Ma, K. Mao, J. Xue, Z. Chen, Z. Chen, H. Zhang
State Key Laboratory of Environmental Geochemistry, Institute of Geochemistry, Chinese Academy of Sciences, Guiyang, 550081, China
E-mail: maokang@mail.gyig.ac.cn
[d] Q. Zhang
College of Civil Engineeing, Tongji University, Shanghai, 200092, China
[e] W. Du
Yunnan Provincial Key Laboratory of Soil Carbon Sequestration and Pollution Control, Faculty of Environmental Science & Engineering, Kunming University of Science & Technology, Kunming, 650500, China

Supporting information for this article is available on the WWW under https://doi.org/10.1002/chem.202403760

electrochemical, mass, mechanical, and other signals.[19] With the emergence of nanotechnology, various novel nanomaterials with excellent optical and electrical properties, such as metal nanoparticles (MNPs), molybdenum disulfide nanosheets (MoS_2), carbon nanotubes (CNTs), graphene, metal-organic framework (MOF) materials, oxide semiconductor materials, and organic fluorescent dyes, have been developed,[20] and various new electrochemical sensors and optical sensors have been developed using these nanomaterials. Sensors have been employed extensively for the detection of heavy metals,[21] pesticides, nucleic acids, antibodies, and pathogens,[22] and they have been shown to be appropriate for applications in environmental monitoring,[23] food safety,[24] agriculture,[25] and medicine.[26]

Among these materials, MOFs constitute a class of periodic network crystal materials characterized by porous structures, which have several advantages, including high specific surface areas, tunable pore structures, versatility, and ease of modification.[27] Additionally, they can be doped with other nanomaterials to form composite materials that are suitable for constructing Hg^{2+} sensors. This provides a novel strategy for addressing the challenge of on-site Hg^{2+} detection, which has long been elusive due to the low concentrations and rapid changes in Hg^{2+} levels and due to a lack of cost-effective methods. Yang et al.[28] utilized selenium-functionalized MIL-101 for the detection of Hg^{2+} in coal-fired power plants, achieving a detection limit as low as 3.5 ng/L. In 2023, Soni et al.[29] investigated the correlations among the synthesis process, structure, and properties of MOFs and explored the utilization of MOFs for the detection of Hg^{2+} in contaminated water sources. These studies indicate that MOF sensors exhibit outstanding analytical performance and potential for applications in the detection of Hg^{2+}.

Although advances in Hg^{2+} sensor development are discussed in several reviews,[30] these publications mainly introduce sensing mechanisms involving DNA enzymes and nanomaterials for Hg^{2+} detection, without specifically discussing the sensors from the perspective of MOFs.[31] Furthermore, there are numerous reviews on MOFs that focus primarily on the detection and removal of pesticide residues, antibiotics, mycotoxins, bio-molecules, phenolic compounds, and heavy metals.[30,32] However, no detailed summary of the progress in the detection of Hg^{2+} is available. For instance, in 2023, Soni et al.[29] reviewed the mechanism of Hg^{2+} detection through nitrogen-, oxygen-, and sulfur-containing functional groups. They explored this from the perspectives of MOF synthesis methods, pore structure, functionality, and chemical properties, as well as the factors influencing MOFs in Hg^{2+} sensing technology. These factors include the stability, recyclability, and selectivity of MOFs, pH, cost, reproducibility, and toxicity. Nevertheless, the mechanism of signal generation during Hg^{2+} detection, the principle of signal amplification, and the progress that has been made in the development of portable integrated equipment for Hg^{2+} detection using MOF sensors were not detailed.

Hence, this work provides a comprehensive overview of the latest advances in MOF-based sensing technology for the detection of Hg^{2+}. It begins by introducing the types and characteristics of MOFs utilized for Hg^{2+} detection, focusing on their synthesis, structure, and properties. Subsequently, the discussion shifts to the progress that has been made in the development of Hg^{2+} detection sensors that employ MOFs, with a particular emphasis on the recognition elements for

Mr Wei Ma is a Master candidate in biochemical engineeing at Hubei Minzu University and is jointly cultivated at the Institute of Geochemistry, Chinese Academy of Sciences. His research focuses on the development of nanosensors for detecting environmental pollutants.

Dr Kang Mao got his PhD degree from Peking University in China and now works as the Associate Professor in Institute of Geochemistry, Chinese Academy of Sciences. His research interest focus on micro/nanosensor for environmental and public health. As first author and corresponding author, he published over 30 peer-review articles on the top journals, such as Environment Sci Technol, Anal Chem, Water Res, TrAC and Biosens Bioelectron, and the H index is 30. Now he is the Associate Editor of Frontiers in Bioengineering and Biotechnology (JCR Q1) and selected as a member of the Youth Innovation Promotion Association of CAS.

Dr. Dong-shan Xiang, a professor from the School of Chemistry and Environmental Engineeing at Hubei Minzu University, is a mentor for postgraduate students. He has been committed to teaching and scientific research in the fields of analytical chemistry and soil environmental analysis. He has made remarkable contributions to the detection and treatment of heavy metals and organic environmental pollutants in soil.

Hg^{2+} and the response signals they generate. The article highlights several MOF-based sensors designed for signal amplification to enhance sensitivity, as well as those engineered for device integration to ensure portability and miniaturization. Finally, it addresses current challenges related to Hg^{2+} detection sensors based on MOFs and outlines potential future directions for sensor development.

2. Synthesis, Structure and Properties of MOFs used in Hg Detection

MOFs are composed of central metal ions, organic ligands, and linkers,[33] as shown in Figure 1(a). The conjugated basic centres within the organic ligands serve as the organic linkers in MOFs. By varying the central metal ions and organic ligands during synthesis, MOFs with distinct structures and properties can be produced.[34] Despite the availability of numerous MOFs, the primary MOFs utilized for Hg^{2+} detection are the Materials Institute Lavoisier (MIL) frameworks, the University of Oslo (UIO) frameworks, and the zeolitic imidazolate frameworks (ZIFs) with acidic molecular sieve skeletons. A series of MOFs are detailed in Table 1. In the following text, the synthesis processes, structures, and properties of these three types of materials are discussed, and a succinct overview of their respective advantages is provided in the context of constructing Hg^{2+} detection sensors.

2.1. UIO MOFs

A UIO MOF is a crystalline material with a periodic network structure, and the preparation method involves mainly solvothermal synthesis, which is based primarily on the reaction of carboxylate and zirconium salts.[37] The spatial structure of a UIO MOF is shown in Figure 1(b). Ghosh et al.[38] prepared a UiO-66-like MOF material (IITG-5) by substituting benzodithiophene-2,6-dicarboxylic acid for terephthalic acid in solvothermal synthesis. The specific surface area of IITG-5 was found to be 1228 m^2/g, with a pore volume of 0.6 cm^3/g and an average pore radius of 10.8 Å. Taher et al.[39] synthesized NH_2-UiO-66 with 2-aminoterephthalic acid as an organic ligand, which features octahedral and tetrahedral structural voids. Thermal stability studies indicated that IITG-5 exhibits exceptional thermal stability below 390 °C, making it suitable for construct-

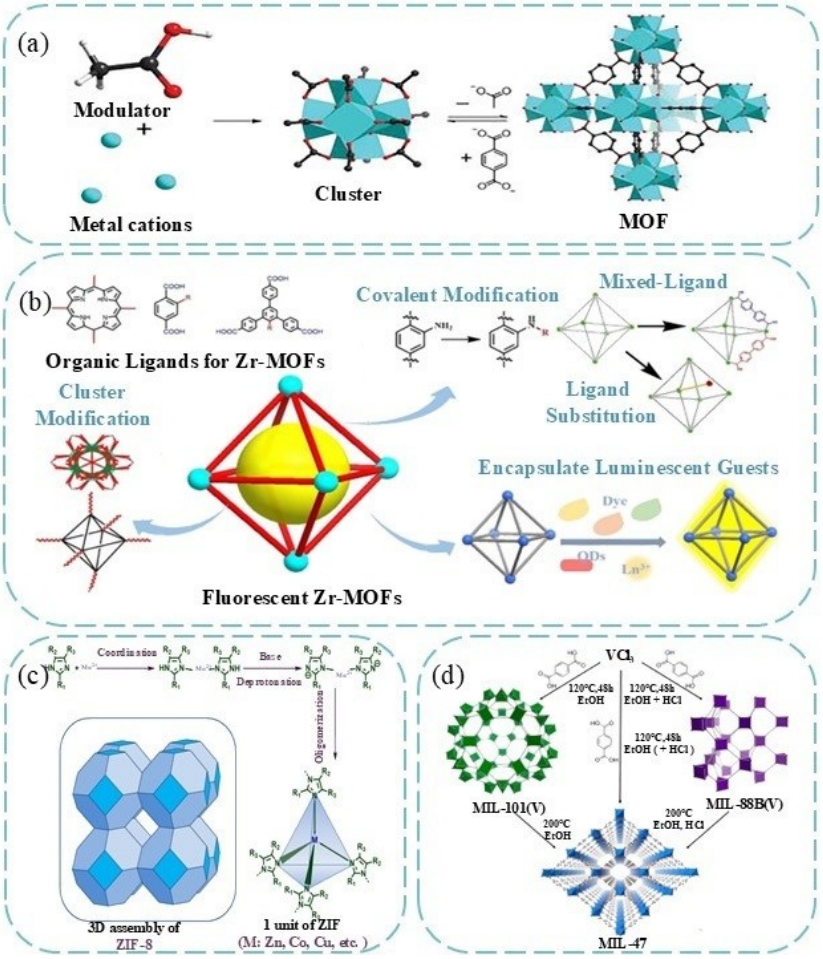

Figure 1. (a) MOF material composition and (b), (c) and (d) synthesis processes and spatial structures of UIO, ZIF and MIL MOFs, respectively (modified from Soin et al[29,35] and Wang et al[36]).

Table 1. MOF –based sensor for Hg^{2+} detection.

Category	Central ion	Organic ligands	Synthesis	Recognition	Signal	Detection range (μ M)	LOD (μ M)	Sample	Ref
Ag-MOF@chitosan@AuNPs	Ag	terephthalic acid	sonication chemistry	T-rich aptamers	fluorescence and electrochemistry	3.0×10^{-7}~1.0	6.6×10^{-8}	tap water and lake water	[55]
DNA–H1@Ru-MOFs@GCE	Ru	1,3,5-phenyltriic acid	electrochemistry	T-rich aptamers	fluorescence and electrochemistry	1.0×10^{-9}~1.0×10^{-3}	3.2×10^{10}	sea water	[56]
Zr-MOF	Zr	benzo[1,2-b:4,5-b′] dithiophene-2,6-dicarboxylic acid	solvothermal heat	thiophene ring	fluorescence	/	5.0×10^{-3}	aqueous solution	[57]
NH_2-MIL-101(Fe)@CdTe QDs	Fe	2-aminoterephthalic acid	solvothermal heat	T-rich aptamers	smartphones	1.2×10^{-4}–1.222	9.1×10^{-5}	lake water, pork, fish and urine	[58]
Tb-MOF	Tb	4,4′,4″-S-triazine-1,3,5-triyltri-p-aminobenzoic acid	solvothermal heat	melamine group	fluorescence	/	4.4×10^{-3}	river water and tap water	[59]
Zn-MOF	Zn	5-aminoisophthalic acid	solvothermal heat	carboxyl	fluorescence	/	0.1243	waste water	[48]
Zr-MOF@AgNC	Zr	2-aminoterephthalic acid	solvothermal heat	sulfhydryl	smartphones	10~5.0×10^{3}	1.8×10^{-3}	nori	[18b]
Zn-MOF	Zn	5-aminoisophthalic acid 4,4′ aziridine	solvothermal heat	pyridine, azo and amino groups	fluorescence	/	1.0×10^{-8}	sea water and tap water	[60]
AuNC/MIL-68(In)-NH_2/Cys	In	2-aminoterephthalic acid	solvothermal heat	sulfhydryl	paper-based microfluidic	5.0×10^{-3}~50	6.7×10^{-6}	lake water and tap water	[61]
AuNC@Ce-MOF	Ce	terephthalic acid	solvothermal heat	AuNC	fluorescence	0.6~2.5×10^{3}	0.2	waste water	[18c]
FA/NH_2-UiO-66	Zr	amino terephthalic acid	solvothermal heat	imine group	fluorescence	1.0×10^{-4}~40	8.85×10^{-5}	sewage	[42]
2D-MOF	/	5-borondiphthalic acid	solvothermal heat	boric acid functional group	fluorescence	0.1~40	4.83×10^{-3}	tap water and sea food	[62]
Fe-MIL-88NH_2/AuNC	Fe	2,5-dihydroxyterephthalic acid	solvothermal heat	sulfhydryl	smartphone	2.0~3.0×10^{4}	7.0	waste water	[63]
CDs/AuNC@ZIF-8	Zn	dimethylimidazole	solvothermal heat	AuNC	fluorescence	3.0~30	1.0	tap water and river water	[50]
2DMOF@S_2/Fe_3O_4@Ag@OPD@S1	/	TCPP	solvothermal heat	T-rich aptamers	SERS	1.0×10^{-6}~1.0×10^{4}	1.36×10^{-7}	river water	[64]
Pd-MOF@GN	Pb	p-phenylenediamine	microwave radiation	Pb	colorimetric and electrochemical	2.0×10^{-2}~2.0×10^{3} 4.5×10^{-2}~2.5×10^{2}	1.2×10^{-2}	river water	[18a]
Eu-MOF	Eu	2-pyridine-4-yl-3H-benzimidazole-5-carboxylic acid	solvothermal heat	benzimidazole	smartphone	0.1–1.0	3.4×10^{-2}	tap, lake and sea water	[65]
AuNP@Fe-TCPP-MOF	Fe	TCPP	solvothermal heat	AuNP	colorimetry	2.0×10^{-4}–4.0×10^{-4}	1.03×10^{-4}	tap water and river water	[66]
AuNP-NH_2-UiO-66	Zr	2-aminoterephthalic acid	solvothermal heat	AuNP	smartphone	0.01~0.1	5.4×10^{-3}	tap water	[39]
Al-MOF	Al	terephthalic acid	solvothermal heat	bis-(4(dimethyl amino) phenyl) methionine	thiamine Al/MOF monitor (TAM)	2.0×10^{-3}~2.1	4.3×10^{-3}	water and cosmetics	[67]

Table 1. continued

Category	Central ion	Organic ligands	Synthesis	Recognition	Signal	Detection range (μ M)	LOD (μ M)	Sample	Ref
BTC–Eu-BDC-NH_2-MOF	Eu	2-aminobenzoic acid and 1,3,5-benzenetricarboxylic acid	sonication chemistry	amino	colorimetry	0.0~0.04	6.7×10^{-2}	tap water	[68]
Au@NH_2-MIL-125(Ti)	Ti	2-aminoterephthalate	solvothermal heat	amino	colorimetry	1.0×10^{3}~5.0×10^{3}	1.0×10^{2}	tap water	[69]
Cu-MOF@GCE	Cu	polyvinylpyrrolidone	solvothermal heat	hydroxyl and amino	electrochemistry	0.1~50	6.33×10^{-5}	tap water and canned tuna	[70]
Carbon hybridization Zr-MOF@GCE	Zr	2-aminoterephthalic acid	solvothermal heat	T-rich aptamers	electrochemistry	/	0.5	vegetable	[71]
Zr-DMBD MOF	Zr	2,5-dimercaptoterephthalic acid	microwave radiation	thiol groups	electrochemistry	2.5×10^{-4}–3.5×10^{-3}	0.05	tap water, lake water and sewage	[72]
Cu-MOF	Cu	1,3,5-benzenetricarboxylic acid	solvothermal heat	T-rich aptamers	electrochemistry	/	4.8×10^{-9}	pure milk	[73]
Ag_2O-NPs@ UiO-66	Zr	1,4-benedicarboxylic acid	solvothermal heat	Ag_2O-NPs	electrochemistry	/	3.0×10^{-3}	lake	[74]

ing Hg^{2+} sensors characterized by large specific surface areas, high porosity, and good thermal and chemical stability.

Zhang et al.[40] synthesized a series of zirconium-based metal-organic frameworks (Zr-MOFs) utilizing amide-functionalized dicarboxylic acid ligands with various side groups. Their findings indicated that these zirconium-based porous crystal materials exhibited excellent hydrolytic stability across a pH range of 3–11 following amide group modification. Additionally, Li et al.[41] employed the porous sites on the surfaces of Zr-MOFs to adsorb AgNCs and used fluorescence resonance energy transfer (FRET) to quench the fluorescence of the AgNCs. They then developed a smartphone-based colorimetric sensor to enable rapid and highly sensitive detection of Hg^{2+}. Similarly, Wang et al[42] synthesized NH_2-UiO-66 via a solvothermal method and modified it with formaldehyde (FA) to fabricate an FA/NH_2-UiO-66 sensor tailored for Hg^{2+} detection.

UIO MOFs synthesized via the aforementioned methods exhibit high specific surface areas, which enhance their adsorption capabilities. A well-developed microporous structure increases the likelihood of surface modification in MOFs. UIO MOFs that are obtained via solvothermal synthesis have high crystal purity, good stability, and modifiable spatial architectures. By selecting diverse organic ligands and reaction parameters, MOFs with distinct structures and properties can be synthesized. Furthermore, the size and morphology of the resulting product can be tailored by manipulating the reaction conditions, such as temperature, pressure, and duration, during the synthesis process. Due to the inherent properties of UIO MOFs, they have significant potential for application in Hg^{2+} detection. Nevertheless, it is important to recognize that the solvothermal synthesis, which involves the use of organic solvents or water as the reaction medium under high-temperature and high-pressure conditions within a reactor, imposes substantial equipment demands and involves severe reaction environment conditions, posing challenges for industrial-scale production.

2.2. MIL MOFs

An MIL MOF is a two-dimensional layered or three-dimensional network-structured crystal material that is synthesized primarily via solvothermal methods. MIL MOFs can be categorized into two groups, as depicted in Figure 1(d): those composed of trivalent metal elements and carboxylic acids, as exemplified by MIL-53 (Fe, Al),[43] and those formed from lanthanide and transition metal elements combined with dicarboxylic acids,[44] such as MIL-53 (Co, Zn), MIL-100 (Cu), MIL-101 (Cr), and MIL-125 (Ti). These materials have advantages such as spatial structural diversity and chemical tunability, rendering them well-suited for applications in materials science and environmental monitoring.

MIL MOFs that are synthesized through the reaction of trivalent metals with carboxylic acids are prevalent MOFs for detecting Hg^{2+}. To investigate the stability and spatial configurations of MIL MOFs throughout this synthesis process, in 2017, Martin Krüger et al.[45] synthesized Al-MOF, a metal-organic framework, by utilizing Al^{3+}/4,4′-benzophenone dicar-

boxylic acid (H_2BPDC) in a DMF/H_2O system. Their findings indicated that Al-MOF remains stable at elevated temperatures and that its spatial network structure can accommodate modifications by recognition or signal groups. Furthermore, Tang et al.[46] employed a solvothermal method to fabricate NH_2-MIL-101(Fe). This material features an almond-shaped spatial structure, and the relative standard deviation (RSD) of its fluorescence intensity was below 4.9%, signifying its excellent fluorescence stability.

A diverse array of MIL MOFs, synthesized from lanthanides, transition metals, and dicarboxylic acids, have been reported for the construction of sensors designed to detect Hg^{2+}. For instance, He et al.[47] employed zinc-free MOFs, such as MIL-53 (Al) and MIL-125 (Ti), to successfully synthesize ZnO nanosheets. Their findings indicated that the properties of the MOF precursors significantly impacted the structural attributes, specific surface area, and oxygen vacancies within the crystalline lattice of the resulting ZnO. Leveraging the spatial architecture of Al-MOFs and their ease of surface tunability, composite sensors with superior photocatalytic activity have been engineered. Furthermore, in addition to carboxylic acid moieties, amino groups exhibit a robust affinity for zinc ions, facilitating the formation of a chemically robust structural framework. In 2020, Jiang et al.[48] synthesized Zn-MOFs featuring a three-dimensional network and an 8.2 Å microporous structure using multi-coordinated 5-amino isophthalic acid as the organic ligand. Their findings indicated that the luminescent Zn-MOF displayed high selectivity and chemical stability in detecting Hg^{2+}.

MIL MOFs exhibit a range of distinctive properties. MIL-53, for instance, has a reversible "breathing" capability that allows for dynamic adjustments to its porosity. MIL-125 and MIL-88B(Fe)-derived heterostructure materials are increasingly employed in the detection and analysis of contaminants in food safety and water environments due to their high porosity, robust water stability, and low biotoxicity. Furthermore, MIL MOFs created using lanthanide and transition metals in conjunction with dicarboxylic acids feature flexible pore structures and expanded surface areas. In contrast, MIL MOFs synthesized from trivalent metal elements and carboxylic acids may have limitations in terms of pore size and specific surface area. Generally, MIL MOFs derived from trivalent metal elements and carboxylic acids exhibit superior thermal and water stability compared to MIL MOFs synthesized from lanthanide transition metals and dibasic carboxylic acids. MIL MOFs synthesized from dicarboxylic acids and lanthanide or transition metals offer a broader array of functional applications, whereas MIL MOFs synthesized from trivalent metal elements and carboxylic acids may present advantages for catalytic reactions. Regarding synthesis costs, the production of MIL MOFs from trivalent metal elements and carboxylic acids is more cost-effective, which facilitates large-scale applications.

2.3. ZIF MOFs

ZIF MOFs represent a class of crystalline materials characterized by highly ordered microporous structures, which are created through coordination bonds between transition metal ions and a variety of organic ligands,[49] as depicted in Figure 1 (c). For instance, Guo et al.[50] prepared ZIF-8 by solvothermal synthesis, coated ZIF-8 onto CDs and AuNCs, and used the action of carboxyl and amino groups to concentrate the ZIF-8 framework building unit and promote the crystallization of ZIF-8 to form CD/AuNC@ZIF-8 composites with dual emission fluorescence. This material, which is prepared under mild synthesis conditions, can allow for the visual recognition of Hg^{2+} with the naked eye.

ZIF MOFs have high specific surface areas, adjustable pore sizes, and stable zeolite topologies.[51] For example, Tu et al.[52] investigated the generation of porous crystal architectures in the synthesis of ZIF materials and developed a versatile model to streamline the synthesis procedure. These porous structures exist in a metastable state and can be altered into a denser polymorph by modifying the synthesis parameters. However, the formation of the ZIF structure can effectively prevent this transition, substantially increasing pore size and stability.

The distinctions among ZIF, UIO, and MIL MOFs are as follows: UIO materials have high thermal and chemical stability along with large specific surface areas. However, their harsh preparation conditions often preclude large-scale production. MIL materials, on the other hand, can have a variety of structures and have tunable porosity, as exemplified by MIL-53, which can undergo reversible changes in porosity. ZIF materials are characterized by their regular pore structures, adjustable pore sizes, high specific surface areas, and zeolite-like topologies, which facilitate surface modification and offer excellent chemical and thermal stability. Nevertheless, their stability in humid environments is subpar, rendering them susceptible to collapse. Each of these three types of materials presents its own set of (dis)advantages in terms of synthesis process, structure, and properties. Therefore, selection considering the specific requirements and environmental conditions for Hg^{2+} detection is needed.

3. MOF Sensors for Hg Detection

An MOF sensor consists primarily of identification elements, signal elements, and conversion elements, along with several auxiliary devices, which can be widely used in Hg detection. MOF-based sensors for Hg detection can be applied over a relatively wide pH range (such as pH 4–10) and have a tolerance to temperature. However, for the detection of other heavy metals, the detection requirements may be more stringent.[53] For example, UIO MOF-based sensors for nickel ions require a pH ranging from 6 to 8. Beyond this range, the structural stability of the MOFs decreases or the interaction with nickel ions is inhibited, resulting in inaccurate detection signals.[54] In this section, we begin by summarizing and examining the MOF sensors designed for Hg^{2+} detection, focusing on the identi-

fication and signal elements. Furthermore, we compare the attributes of various MOF-based sensors. To conclude, we discuss the advance in research on Hg^{2+} sensors, particularly in terms of device integration.

3.1. Recognition Elements of MOF-Based Sensors for Hg Detection

As illustrated in Table 1, the recognition elements for Hg^{2+} can be categorized into three groups: (1) MOFs that inherently possess specific recognition capabilities for Hg^{2+}, which include central metal ions and organic ligand functional groups within the MOFs[34a,75]; (2) MOFs in which these inherent recognition capabilities are significantly improved through MOF modification with auxiliary materials. For instance, the integration of metal nanomaterials with MOFs to create composite materials yields a hybrid that combines the inherent recognition properties of the MOFs with the supplementary recognition functionalities of the metal components[34a,55,76]; (3) MOFs that do not inherently recognize Hg^{2+} but are tailored to specifically target Hg^{2+}, for instance, by incorporating T-rich aptamers.[71] Each of these types of recognition elements is examined in depth below.

The recognition of Hg^{2+} in MOFs is governed primarily by functional groups present in the organic ligands (refer to Figure 2). These groups have the ability to coordinate with Hg^{2+}, resulting in the formation of stable complexes. For instance, Jiang et al.[48] synthesized ZIF MOFs utilizing the carboxylic acid moiety of the 5-aminoisophthalic acid organic ligand for the specific recognition of Hg^{2+}. Anti-interference experiments demonstrate that the constructed sensor generated a rapid fluorescence quenching response upon the addition of Hg^{2+} to aqueous solutions containing interfering ions. Furthermore, functional groups containing sulfur atoms have also been found to specifically recognize Hg^{2+}. Ghosh et al.[38] investigated the synthesis mechanism of new UiO-66 materials in the presence of Hg^{2+}. They found that energy transfer from IITG-5 to Hg^{2+} was dissipated through luminescence. They also confirmed that the fluorescence quenching of IITG-5 occurred due to strong coordination between sulfur atoms in the thiophene ring and Hg^{2+}. Furthermore, it has been established that the nitrogen atom within the amino group is highly electronegative, which leads to the partial ionization of the amino molecule, rendering it nucleophilic. Consequently, Hg^{2+} directly targets the nucleophilic amino group.[77] Xia et al.[59] employed 4,4,4-S-triazine-1,3,5-triaminobenzoic acid as an organic ligand to synthesize a series of lanthanide MOFs. They utilized the interaction between the nitrogen atoms in the triazine and imine moieties with Hg^{2+} to detect the presence of Hg^{2+}. Furthermore, the recognition of various metal ions, including Hg^{2+}, within MOFs has been documented. For instance, Liu et al.[18a] revealed that the amalgamation of Hg^{2+} and Pd ions endows Pd-MOF@GN systems with oxidase-like (OXD) activity. This activity facilitates the oxidation of the substrate TMB, resulting in a colour change, and also promotes

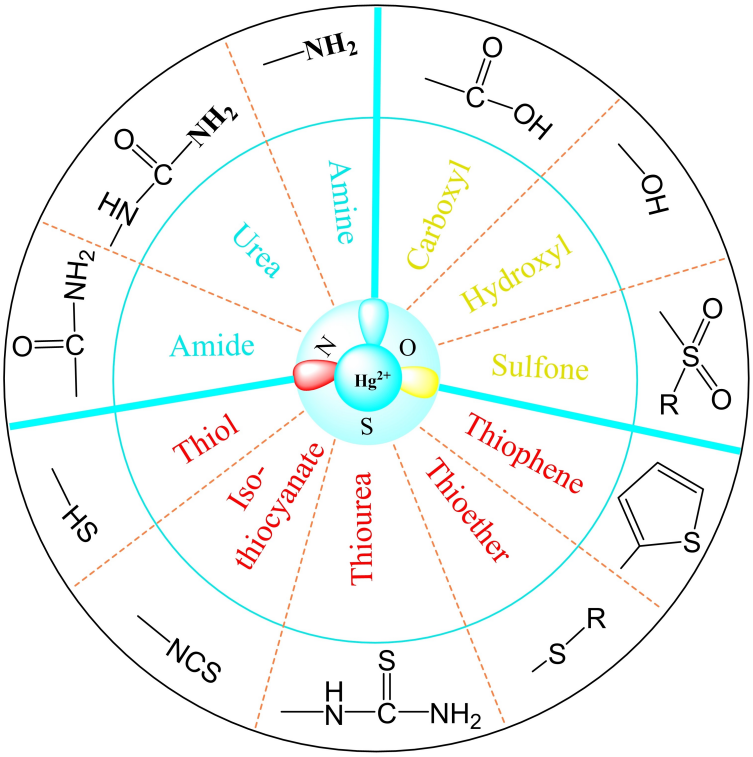

Figure 2. Functional groups involved in Hg detection and identification elements (summarized in Table 1).

the oxidation of OPD to yield OPD ox, thereby generating a distinct anodic signal. Consequently, a dual-mode colorimetric and electrochemical sensor for the detection of Hg^{2+} can be successfully established.

To enhance the precision of detecting low-level Hg^{2+}, hybrid structures composed of nanomaterials and MOFs can be developed with MOFs as the recognition elements. Additionally, these MOFs can be tailored for Hg^{2+} recognition by metal nanomaterials that accumulate Hg^{2+}, thereby intensifying the surface modification of the MOFs. The amalgamation of Hg^{2+} on the surfaces of gold nanoparticles (AuNPs) or gold nanoclusters (AuNCs) triggers the catalytic activity of AuNPs or diminishes the intrinsic fluorescence of AuNCs.[18c,66] For example, in 2020, Wang et al.[66] immobilized AuNPs on the surfaces of Fe-TCPP-MOFs to leverage the reductase activity of gold amalgam in aqueous solution, taking advantage of the uniform cavity structure and high porosity of the MOFs. This ensured a uniform distribution of AuNPs across the cavity surfaces, enhancing the likelihood that Hg would interact with methylene blue. In a separate study, Zhang et al.[18c] employed the porous structure on the surfaces of Ce-MOFs to enhance the local Hg^{2+} concentration via the adsorption capabilities of the Ce-MOFs, which resulted in the quenching of the autofluorescence of AuNC/Ce-MOFs due to specific recognition between Au and Hg, as depicted in Figure 3(c). Similarly, Wu et al.[61] utilized cysteine to tailor a fluorescence sensor composed of AuNC/MIL-68(In)-NH_2 and developed a microfluidic paper-based analytical device (μPAD) for the rapid, cost-effective, and visual detection of Hg^{2+}. In addition to gold nanoparticles, reports have emerged regarding the use of other noble metal nanomaterials in MOFs. For example, in 2022, Li et al.[18b] deposited AgNCs onto the surfaces of UiO MOFs via electrostatic attraction, inducing fluorescence resonance energy transfer (FRET) that resulted in the quenching of Zr-MOF fluorescence, as depicted in Figure 3(b). The sulfhydryl groups on the AgNC surfaces reacted with Hg^{2+} to form a complex, which resulted in the detachment of the AgNC from the Zr-MOF surfaces and the restoration of fluorescence.

Furthermore, to increase the specificity of Hg^{2+} detection, additional recognition elements can be incorporated into MOFs, augmenting the inherent functional group-specific recognition capabilities of the MOFs.[78] For instance, T-rich aptamers can be introduced, which are capable of selectively capturing Hg^{2+} through mismatch pairing to form a stable T-Hg^{2+}-T structure. This addition enhances selectivity and reduce interference in the Hg^{2+} detection method, as depicted in Figure 3(a).[79] Liu et al.[80] investigated challenges related to overlapping and indistinguishable redox signals from Pb^{2+} during the detection of Hg^{2+} in complex environmental settings. Anthraquinone-2-carboxylic acid (AQ)-tagged single-stranded DNA served as complementary DNA, binding with ferrocene (Fc)-marked Hg^{2+} aptamers and methylene blue (MB)-labelled Pb^{2+} aptamers. The current signal from air quality (IAQ) was utilized as an internal reference, and the signals of IAQ/IFC and IAQ/IMB were employed to identify the presence of Hg^{2+} and Pb^{2+} in soil, paddy soil, and crayfish. Building upon this approach, Wang et al.[71] doped UiO-66 MOFs with large specific surface areas with carbon tubes as electrode modification materials (UiO-66-CNTs) to load complementary chains of T-rich aptamers. Hg^{2+} and Pb^{2+} aptamers were hybridized to the surface complemen-

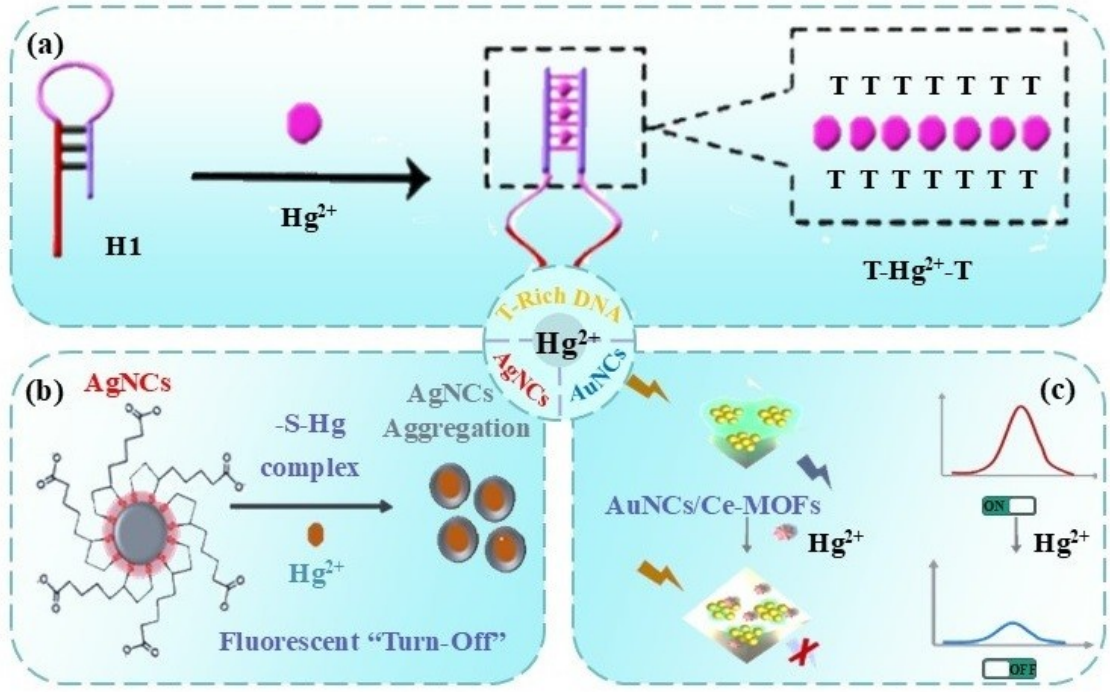

Figure 3. (a) Hybridization of T-rich hairpin DNA and (b), (c) MOF identification of Hg^{2+} by AgNC and AuNC (modified from Li et al.,[24] Zhang et al.,[25] and Zhou et al.[79]).

tary strands of UiO-66-CNTs to form m-type functionalized DNA complexes, and the stable structures of the UiO-66-CNTs prevented the DNA from being affected by environmental factors.

In the context of MOFs employed for the detection of other heavy metals, the mechanisms underlying the recognition elements principally encompass ion exchange, electrostatic adsorption, and coordination of metal ions.[81] Taking lead ions as an example, recognition presumably operates on the basis of an ion exchange mechanism. Specifically, lead ions replace the heavy metal ions within the MOFs structure, consequently giving rise to modifications in the crystal structure and concomitant signal fluctuations.[82] Chromium (VI) ion detection may involve complexation reactions with functional groups such as carboxyl groups on the MOF surface, thereby effecting changes in the electrical properties of the material for detection.[83] In comparison with Hg detection, the interaction specificity between these heavy metals and MOFs is tenuous, and it routinely demands the employment of MOFs that are either modified or possess specially engineered structures to augment selectivity.Consequently, specific MOFs manifest remarkable selectivity for Hg. Specifically, MOFs incorporating Hg-specific recognition moieties are capable of effectively discriminating Hg from other metal ions within intricate environments. Nevertheless, the selectivity for other heavy metals is comparatively inferior. For instance, in the presence of multiple heavy metals, MOFs constructed on the basis of conventional organic ligands may be subject to interference from zinc ions, and cadmium ions during the detection of lead ions.[84] This is because these ions also interact with the MOFs, albeit with marginally discrepant interaction modalities and intensities. By contrast, the specific binding of Hg alleviates interference from other elements to a certain extent. For other heavy metals, as illustrated in Table S1. the detection limits of various MOF-based sensors are approximately at the μM level.[85] For example, the detection limit of Cu^{2+} based on bipyridine-MOF is 1 μM, which is higher than that of Hg.[86] This is because Hg could strongly bind with specific functional groups, while the affinity between other heavy metals and MOFs are weaker.

In summary, Hg^{2+} recognition components include mainly metal ions and organic functional groups in MOFs, metal nanomaterials, and T-rich aptamers. The detection of Hg^{2+} in MOFs depends on the formation of coordination bonds between the unsaturated valence electrons of organic ligands, typically involving non-metal atoms such as nitrogen, oxygen, and sulfur and Hg^{2+}. This method results in excellent stability and rapid detection times in real scenarios. However, recognition efficacy is often compromised in the presence of other heavy metals, which impacts the precision.

In comparison, the interactions between metal ions and Hg^{2+} within MOFs are seldom documented, potentially because the interactions among metal ions during Hg^{2+} detection cause overlapping signals that are challenging to discern. Furthermore, individual recognition groups are susceptible to interferences in complex environments; therefore, further enhancement in their specificity is needed. As a specialized recognition element, the T-rich aptamer creates a stable T-Hg^{2+}-T structure with Hg^{2+}, markedly enhancing the anti-interference capabilities of Hg^{2+} detection sensors. Nevertheless, aptamers, being nucleic acids, are susceptible to the influence of environmental factors such as pH and temperature during detection. Additionally, to detect Hg^{2+} at low concentrations, metal nanoparticles and MOFs can be synthesized into hybrid materials. In these composites, MOFs serve as both recognition elements and as a means for accumulating Hg^{2+}, thus facilitating identification. Moreover, dual recognition elements enhance the accuracy and stability of Hg^{2+} detection. However, the preparation processes of these hybrid materials have drawbacks such as poor repeatability, complex procedures, and high costs, making industrial-scale production of Hg^{2+} detection nanomaterials difficult to achieve.

3.2. Signal Elements in MOF Sensors for Hg Detection

Based on Table 1, Hg^{2+} sensors based on MOFs can be categorized into optical sensors, electrochemical sensors, and dual-signal sensors. Optical sensors, which encompass fluorescence and colorimetric types, are used most often in Hg detection. Electrochemical sensors leverage the porous nature of MOFs and incorporate nanomaterials to boost the electrochemical properties of these materials. However, the research on MOF electrochemical sensors for Hg^{2+} detection is relatively limited. Dual-signal sensors, whether fluorescence/colorimetric or photoelectric, can markedly reduce background signals during Hg^{2+} detection and are anticipated to be integrated with portable sensors for in-field Hg^{2+} detection. In this section, we examine Hg^{2+} detection via these three types of MOF sensors.

3.2.1. Optical MOF Sensors for Hg Detection

(1) Fluorescence MOF Sensors for Hg

Fluorescence sensing technology capitalizes on the capacity of recognition elements to specifically bind target substances, which induces alterations in the fluorescence signals of the fluorophores, including phenomena such as quenching and recovery.[87] This method results in high sensitivity, excellent selectivity, and rapid response times. Additionally, it features straightforward operating procedures, minimal background signal interference, non-destructive detection capabilities, and the ability to simultaneously detect multiple targets, and it is cost-effective in detection.[88] Fluorescence sensors for Hg^{2+} detection based on MOFs can be categorized into three types, depending on the source of fluorescence signal: MOFs that exhibit intrinsic luminescent properties without the need for additional fluorescent substances; MOFs that are not fluorescent on their own but become fluorescent when combined with other fluorescent materials; and MOFs that possess both their own fluorescent signals and those from other fluorescent molecules.

At present, the fluorescence sensing of Hg^{2+} based on MOFs is driven mainly by the fluorescence signals of MOFs. Xia et al.[59] developed an Hg^{2+} sensor by employing a luminescent lanthanide MIL MOF material, in which the melamine moiety within the organic ligand served as the recognition element. Its interaction with Hg^{2+} resulted in pronounced fluorescence quenching of MOF luminescence. The sensor's detection limit for Hg^{2+} was determined to be 4.4 nM. Like the fluorescence attributes of MIL MOFs, the luminescent properties of UIO MOFs are excellent. For instance, Subhrajyoti Ghosh et al.[38] synthesized UiO-66-like materials exhibiting blue fluorescence using a solvothermal method. The resultant IITG-5 material was then coated onto a strip of filter paper. Utilizing this setup, two antibiotics-NFZ and NFT-in a methanol medium, as well as Hg^{2+} in an aqueous solution, were simultaneously detected. The response time achieved was as short as 1 min at nM-level concentrations.

Furthermore, by employing the same organic ligands and varying the metal ion clusters, different luminescent MOFs can be synthesized, each displaying distinct fluorescence intensities. For example, ElTaher et al.[77] synthesized four luminescent MOF materials, each with distinct metal clusters, by utilizing 2-amino terephthalic acid as the organic ligand. These materials were NH_2-Cd-BDC, NH_2-MIL53(Al), NH_2-MIL88(Fe), and NH_2-UiO-66(Zr). The sensors made from these MOFs exhibited detection limits in the micromolar range for Hg^{2+} detection in aqueous environments. However, there were notable differences in their selectivity; specifically, NH_2-Cd-BDC and NH_2-MIL53(Al) outperformed NH_2-MIL88(Fe) and NH_2-UiO-66(Zr), as evidenced by their higher fluorescence quenching responses.

Although some MOFs lack inherent fluorescence, sensors for detecting Hg^{2+} that incorporate other luminescent materials have been documented.[89] For instance, researchers have tailored luminescent nanomaterials that exhibit aggregation-induced emission (AIE) characteristics and affixed them to the surfaces of MOFs. The detection of Hg^{2+} was made possible through alterations in the optical signal, which occurred due to the aggregation of Hg^{2+}. Zhang et al.[18c] synthesized hybrid AuNC@Ce-MOF materials by depositing AuNCs with AIE properties onto the surfaces of Ce-MOFs. During the Hg^{2+} detection, the Ce-MOFs facilitate the aggregation of Hg^{2+}, which in turn induces alterations in the fluorescence intensity of the AuNCs. This innovative material was employed to detect Hg^{2+} in wastewater, in which the material had a linear response range of 6.0×10^{-7} to 2.5×10^{-3} M Hg^{2+} and a detection limit of 2.0×10^{-7} M for Hg^{2+}. In another study, Guo et al.[50] developed a sensor utilizing the fluorescence signals of gold nanoclusters (AuNCs) and carbon dots (CDs) for the detection of Hg^{2+} ions. The preparation of the sensor involved coating CDs and AuNCs with ZIF-8, which resulted in the formation of CD/AuNC@ZIF-8 composites that exhibited dual-emission fluorescence. As the concentration of Hg^{2+} increased, the red fluorescence emitted by AuNCs within the CD/AuNC@ZIF-8 composites was suppressed, whereas the blue fluorescence from the CDs remained constant. This sensor was successfully applied to detect Hg^{2+} in tap and river water samples, with a linear response range of 3.0×10^{-6} to 3.0×10^{-5} M and a detection limit of 1.0×10^{-6} M.

Unlike sensors with double fluorescence signals, sensors for detecting Hg^{2+} based on fluorescence from both MOFs and other fluorescent molecules are seldom reported. In 2022, Lu et al.[63] improved the reliability of AIE for Hg^{2+} detection and minimized background signal interference by modifying AuNCs with fluorescence response with iron (Fe). They then combined these modified AuNCs with the surface of MIL-88 MOFs and integrated equipment to construct an Hg^{2+} detection sensor, as depicted in Figure 4(a). They leveraged the competitive effect of thiram and AuNCs on Hg^{2+} and utilized the red fluorescence of AuNCs at 643 nm as the Hg^{2+} detection signal and the blue fluorescence of MIL-88 NH_2 at 427 nm as the internal control signal. Hg^{2+} detection was achieved through the fluorescence response of Fe-MIL-88NH_2/AuNC based on an "on-off-on" mechanism.

MOF fluorescence sensors leverage the inherent fluorescence of MOFs or that of surface-modified of nanomaterials to enhance the fluorescent properties of the materials. When applied for the detection of Hg^{2+}, MOF fluorescence sensors offer several advantages: they exhibit greater sensitivity, accuracy, and repeatability compared to traditional detection methods. By harnessing the AIE effect, they enable the detection of Hg^{2+} at low concentrations through aggregation, and the dual-emission fluorescence signals provide self-calibration, thereby enhancing the reliability, accuracy, and sensitivity of the method. Some of these fluorescence sensors have been integrated into portable devices that are characterized by rapid detection times, affordability, and the ability to detect multiple targets simultaneously. The sensing platform also has a high degree of automation and portability, indicating significant potential for practical applications.

(2) Colorimetric Sensors for Hg Detection Based on MOFs

Colorimetric sensors leverage the absorption properties of light-absorbing substances to detect variations in the intensity or wavelength of light absorbed, thereby quantifying the concentration of target substances.[90] Certain colorimetric materials have a unique ability to visibly display colour changes,[91] which presents advantages such as rapid response times, ease of operation, low cost, and suitability for integration into compact devices for Hg^{2+} detection. Colorimetric sensors for Hg^{2+} detection can be categorized based on the source of the colorimetric signal into three types: those utilizing MOFs with catalytic activity to facilitate the colour-forming reaction; those in which MOFs lack catalytic activity, necessitating modification with other nano catalytic materials or chromogenic groups; and those that benefit from both the catalytic activity of the MOFs and the chromogenic groups of other nanomaterials.

Most colorimetric sensors for Hg^{2+} detection are governed by the intrinsic catalytic properties of the MOFs that they incorporate. For instance, Zhang et al.[67] developed an MOF sensor that leverages the catalytic activity of a two-dimensional MOF in conjunction with magnetic nanomaterials. The sensor employs Fe_3O_4@Ag@OPD as a signal carrier for the detection of Hg^{2+}. Upon exposure to Hg^{2+}, T-rich hairpin DNA sequences S1

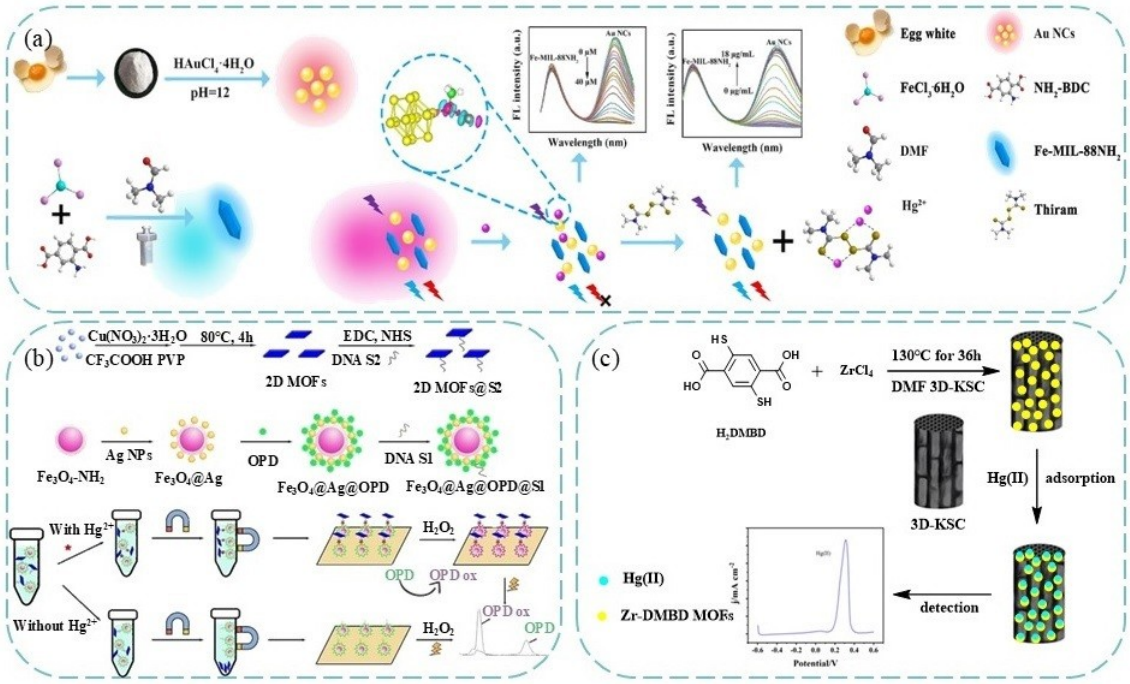

Figure 4. Hg^{2+} detection sensors. (a) Fluorescence sensors (b) Colorimetric sensors and (c) Electrochemical sensors (modified from Lu et al.,[63] Yang et al.,[72] and Wang et al.[66]) based on MOFs.

and S2 undergo conformational changes, forming stable T-Hg^{2+}-T structures. This leads to the ligation of Fe_3O_4@Ag@OPD@S1 and MOF@S2, resulting in the formation of complexes. Following magnetic separation, hydrogen peroxide (H_2O_2) is introduced into the supernatant. The MOFs then catalyse the oxidation of OPD to produce 2,3-diaminylphenazine (OPD ox). In another study, Wang et al.[83] engineered a mixed valence cerium-based MVC–MOF sensor, which incorporated the partial oxidation of Ce^{3+}. The sensor featured a unique interaction with thymine-rich single-stranded DNA (T-rich ssDNA), which adhered to the MVC–MOFs, effectively covering active sites and reducing the catalytic capabilities of the materials. Upon exposure to Hg^{2+}, the T-rich ssDNA bound to the MVC–MOF underwent a conformational change, folding into a distinctive rigid double-stranded DNA (dsDNA) structure. This structural alteration restored the catalytic activity of the MVC–MOF, facilitating the oxidation of TMB to produce the blue oxidized product TMB ox. In an aqueous setting, the sensor demonstrated a robust linear correlation for Hg^{2+} with a detection limit of 10.5 nM. Nonetheless, the addition of hydrogen peroxide (H_2O_2) as an oxidizing agent was necessary during the detection process.[92] However, the susceptibility of H_2O_2 to environmental decomposition poses a significant challenge to the practical application of this colorimetric sensor for in-field Hg^{2+} detection.

MOFs lack inherent catalytic activity; however, catalytic activity has been documented in colorimetric sensors generated from alternative catalytic materials or surface-modified chromophores. For instance, Chen et al.[93] demonstrated that Hg^{2+} can be reduced through a counter coupling reaction on the surfaces of gold films. They also revealed that gold amalgam substantially enhances the activity of peroxidase and catalase gold films. Furthermore, the reduction in the activation energy of gold amalgam during formation is the underlying reason for the promotion of the reactions of peroxidase and catalase. Wang et al.[66] further investigated the practical application of an amalgam for the detection of Hg^{2+}. As illustrated in Figure 4(b), to avoid the aggregation of gold nanoparticles (AuNPs), which could lead to diminished catalytic activity, AuNPs were uniformly embedded within the surface cavities of Fe-TPCP-MOFs. This resulted in the synthesis of a hybrid material that combined AuNPs with MOFs. During the detection of Hg^{2+}, an amalgam on the AuNP surface catalysed the reduction of methylene blue (MB). This resulted in impressively short response times and low detection limits for Hg^{2+}, in tap water and seawater, the response time was as low as 2 seconds, and the detection limit was a low as 103 pM.

In addition to the catalytic properties of MOFs, chromophores on the surfaces of MOFs have also been modified. For instance, Ahmed Radwan et al.[67] immobilized a chromophore with a dim ethane throne-type structure onto the surfaces of Al-MOF micropores. Using this chromophore molecule, they engineered a throne-type Al-MOF (TAM) colorimetric sensor specifically designed for the detection of Hg^{2+}. When exposed to Hg^{2+}, TAM forms a $[Hg\text{-}TAM]^{n+}$ complex, which causes a distinct colour shift from yellow to dark green. This sensor was employed to detect Hg^{2+} in both real water samples and in

cosmetics, achieving a detection limit of 0.8 parts per billion (ppb).

MOF-based colorimetric sensors capitalize on the interactions between MOFs and analytes, which triggers changes in MOF catalytic activity. These changes subsequently affect the colour of a chromogenic substance, thereby enabling the detection of analytes. The applicability of colorimetric sensors for the detection of Hg^{2+} depends primarily on the enzyme-mimetic activity of the MOFs, the surface-modified nano catalytic materials, and the action of chromogenic groups within nanomaterials on chromogenic substrates, which result in colour changes. This method offers several benefits, including rapid response times, heightened sensitivity, excellent selectivity, and minimal signal interference from background substances.

3.2.2. Electrochemical MOF Sensors for Hg Detection

An electrochemical sensor is a device that transduces the concentration or activity of a chemical species into an electrical signal, facilitating the quantitative or qualitative analysis of a target substance through the detection of variations in electrochemical parameters, such as current, potential, or conductivity, between electrodes.[94] Electrochemical sensors are characterized by their high sensitivity, rapid response times, user-friendly operation, cost-effectiveness, and compatibility with miniaturized devices.[95] In this section, we examine the specifics of Hg^{2+} detection via electrochemical sensors and categorize the sensors based on the various classes of MOFs employed.

The most common type of MOF material that is employed in electrochemical sensors for Hg^{2+} detection is MIL MOFs. Cui et al.[56] successfully integrated Ru-MOF with strand displacement amplification (SDA) to develop an electrochemical sensor for the detection of Hg^{2+}. Through SDA, T-rich aptamers were transformed into target DNA, which then hybridized with hairpin DNA–H1. This interaction facilitated the formation of a quadruple helix structure that captured hemoglobin and released oxygen quenchers. These quenchers subsequently acted on the electrodes, resulting in the attenuation of the electrochemical signal. For the detection of Hg^{2+} in seawater, the sensor exhibited a detection limit of 3.2×10^{-4} pM. To ensure that the accuracy of Hg^{2+} detection is not compromised by the aggregation of metal nanoparticles, Liu et al.[55] synthesized a Pb-MOF by establishing Pb–NH_2 bonds with p-phenylenediamine, which effectively prevented the aggregation of Pb nanoparticles. An enhancement in the electrochemical signal was achieved with the use of graphene oxide (GO). Additionally, the Pb-MOF was grown in situ on polyvinylpyrrolidone (PVP)-functionalized graphene nanosheets, which resulted in the formation of Pb-MOF@GNs. The redox properties of the Pb-MOF@GNs and Hg^{2+} systems were explored using electrochemical voltammetry. The oxidation of o-phenylenediamine (OPD) to OPD ox yielded a distinct anodic signal, and the changes in the oxidation peak current within the system were compared. The sensor exhibited excellent accuracy, reliability, and stability in the detection of Hg^{2+}. In addition, research has been conducted on enhancing the electrical properties of MOFs, such as their conductivity and cycling, in electrochemical sensors. Singh et al.[70] employed polyethylene pyrrolidone (PVP) as an organic linker to enhance the stability and electron transfer rate of MIL-100 (Cu). The adsorption of Hg^{2+} was facilitated by the -OH and -NH functional groups present in the linker molecule.

In addition to MIL MOFs, sensors for detecting Hg^{2+} constructed from UIO MOFs have been reported. For instance, Yang et al.[72] synthesized thiol-functionalized MOFs using Zr (IV) and 2,5-dimercaptoterephthalic acid (Zr-DMBD), which were subsequently integrated with a three-dimensional kenaf stem-derived carbon (3D-KSC) to create a novel nanocomposite material. This material was designed for the fabrication of electrochemical sensors capable of detecting Hg^{2+}. As depicted in Figure 4(c), the Zr-DMBD MOF was evenly distributed across the 3D-KSC surface. The presence of thiol groups facilitated the enrichment of Hg^{2+} at the electrode, altering the electrical signals of the tri-electrode system to enable both qualitative and quantitative analysis of Hg^{2+}. When applied to the detection of Hg^{2+} in tap water, lake water, and sewage, the sensor exhibited a linear response in range of 0.25 μM to 3.5 μM with a detection limit of 0.05 μM for Hg^{2+}. Moreover, the Zr-DMBD MOF/3D-KSC nanocomposite demonstrated excellent stability, repeatability, and the ability to effectively eliminate Hg^{2+} from real wastewater samples. In practical applications, the sensor exhibited robust anti-interference capabilities for Hg^{2+} detection.

In electrochemical sensors, MOFs are employed as the electroactive components, and electrodes are used as the transducers to detect target substances. This is achieved by inducing changes in potential or current within the electrical signalling substances released during the identification of the target substances. MOF-based electrochemical sensors designed for the detection of Hg^{2+} not only exhibit excellent anti-interference capabilities, reproducibility, reliability, repeatability, and applicability but also offer advantages such as rapid detection, cost-effectiveness, heightened sensitivity, low detection thresholds, ease of operation, and the potential for automation and miniaturization. Nevertheless, in comparison with optical sensors, less research has been conducted on Hg^{2+} electrochemical sensors. This is attributed to the inherent drawbacks of the MOFs used for Hg^{2+} detection, such as conductivity issues, limited functionality, and cycling instability.

3.2.3. Dual-Signal MOF Sensors for Hg Detection

Electrochemiluminescence (ECL) involves the activation of electrochemically active substances, which triggers an electrochemical reaction. This reaction generates active intermediates and excited luminescent species, which result in the emission of light signals. Sensors developed using this technology have several advantages, including affordability, heightened sensitivity, straightforward control mechanisms, and uncomplicated operational requirements. Consequently, they have been applied extensively in the detection of environmental pollutants

and in ensuring food safety.[96] In this section, we categorize and discuss Hg^{2+} dual-signal MOF sensors, focusing on their fluorescence, electrochemiluminescence, colorimetric, and electrochemical signals. We also examine the mechanisms involved in the generation of these signals in MOF sensors for Hg^{2+} detection.

The dual fluorescence and electrochemiluminescence properties of MOF-based sensors have been documented for the application of these materials in the detection of Hg^{2+}. For example, Liu et al.[55] employed streptavidin to conjugate chitosan (CS) with gold nanoparticles (AuNPs), forming a hybrid composite designated as Ag-MOF@CS@AuNPs. This composite adhered to the surfaceS of Ag-MOFs. In the absence of Hg^{2+}, streptavidin was bound to the electrode, which led to a reduction in the fluorescence intensity of the Ag-MOF as the biotin-modified T-rich aptamer specifically bound to streptavidin. Upon the introduction of Hg^{2+}, the T-rich aptamer dissociated from the electrode surface, causing a gradual decrease in the amount of streptavidin bound to the electrode. Consequently, the electrochemiluminescence intensity of Ag-MOF@CS@AuNPs increased.

To further enhance the specificity of the Hg^{2+} detection process, a dual-signal sensor that incorporates fluorescence and electrical signals, based on short-chain nucleic acid sequences modified with MOFs, was developed for the detection of Hg^{2+}. For instance, Cui et al.[56] developed a dual-signal sensor DNA–H1@Ru-MOFs@GCE, which was modified with T hairpin aptamers. To prevent mutual interference between Hg and silver ions during detection, C-rich aptamers were incorporated to mask signal interference from silver ions in the detection of Hg^{2+}. Upon the introduction of DNA polymerases, restriction enzymes, and deoxyribonucleotides, a strand displacement amplification reaction was triggered, transforming the initial Hg^{2+} detection process into an assay for target DNA (tDNA). The hairpin DNA H1 rapidly unfolded to pair with tDNA, forming base-complementary double-stranded DNA. Concurrently, the G-rich hairpin DNA H1 assembled into a G-quadruplex structure via Hoogsteen base-pairing, capturing haemoglobin and causing the release of dissolved oxygen from haemoglobin. This led to a decrease in the electrical signal of Ru-MOFs@GCE and the quenching of the fluorescence signal of $Ru(bpy)_3^{2+}$ by the released oxygen.

In addition to fluorescence and electrochemiluminescence signals, dual-signal Hg^{2+} detection sensors that combine fluorescence with electrical signals have been reported. Furthermore, colorimetric and electrochemical dual-signal sensors, which leverage the catalytic properties of MOFs, have been developed for the detection of Hg^{2+}. For instance, to enhance the precision and dependability of Hg^{2+} detection. Liu et al.[18a] engineered a dual-signal MOF sensor by utilizing colorimetric and electrochemical detection methods for Hg^{2+} without hydrogen peroxide supplementation. The synthesis of the Pd-MOF@GN hybrid material was achieved in situ on graphene nanosheets functionalized with polyethylene pyrrolidone (PVP). The amalgamation of Hg^{2+} with Pd-MOF@GN resulted in oxidase-like (OXD) activity. As depicted in Figure 5(b), this OXD activity catalysed the transformation of 3,3′,5,5′-tetramethylbenzidine (TMB) and o-phenylenediamine (OPD), inducing colour changes in chromogenic substrates and enhancing electrical signals during the oxidation process of OPD—without the introduction of H_2O_2.

Furthermore, optical dual-signal Hg^{2+} detection MOF sensors that utilize both fluorescence and colorimetry have been reported. For instance, Li et al.[18b] attached AgNCs to the surfaces of UIO MOFs through electrostatic adsorption, leading to FRET fluorescence quenching, to construct a fluorescence colorimetric dual-signal Hg^{2+} detection sensor. The sulfhydryl groups on the surfaces of AgNCs interacted with Hg^{2+} to form a complex, the AgNCs detached from the surfaces of Zr-MOFs to restore Zr-MOF fluorescence, and the detached AgNCs could act on chromogenic substances to produce visual colour changes, as shown in Figure 5(a). This material was used for the detection of Hg^{2+} in laver, and the sensor showed good sensitivity at 0.01–0.5 μg/L with a detection time of 10 min. At the same time, by capturing the fluorescence colour changes at different Hg^{2+} concentrations, a visual colorimetric method based on smartphones was established. MOF optical dual-signal sensors enabled signal amplification and visualization, and when combined with portable devices that are easy to integrate, they are expected to enable on-site Hg^{2+} detection.

The MOF dual-signal sensing strategy represents an innovative approach that integrates optical and electrical signals. In this technology, by utilizing MOFs as the sensing elements, target analytes are detected by monitoring alterations in fluorescence, colorimetric, electro chemiluminescent, and electrochemical signals. Specifically in the detection of Hg^{2+}, MOF dual-signal sensing technology leverages the enhanced luminous efficiency and the ability of MOFs to aggregate Hg^{2+} to enable the detection of this ion at low concentrations. The dual-signal detection mechanism further minimizes background signal interference, facilitating rapid, highly sensitive, and selective identification of Hg^{2+}. Despite these advances, research into dual-signal Hg^{2+} detection using MOF sensors remains confined to laboratory settings and has not yet been translated into field applications for real-time Hg^{2+} detection.

3.3. Portable Device-Based MOF Sensors for Hg Detection

In recent years, portable integrated devices—devices that combine multiple functional components into a single unit to fulfil a particular purpose or function—have garnered significant attention,[97] as they facilitate the transition from laboratory to field environmental testing.[98] A range of integrated devices, including gas detectors, water quality analysers, metal detectors, mobile phones, and microfluidic systems, have been developed and are now extensively utilized across the environmental, medical, food safety, and agricultural sectors.[99] This section provides an overview of portable devices for Hg, including mobile phones, microfluidic devices, and paper-based devices. However, there is lack of literature discussing the application of MOF sensors within these portable integrated systems for the detection of Hg^{2+}.

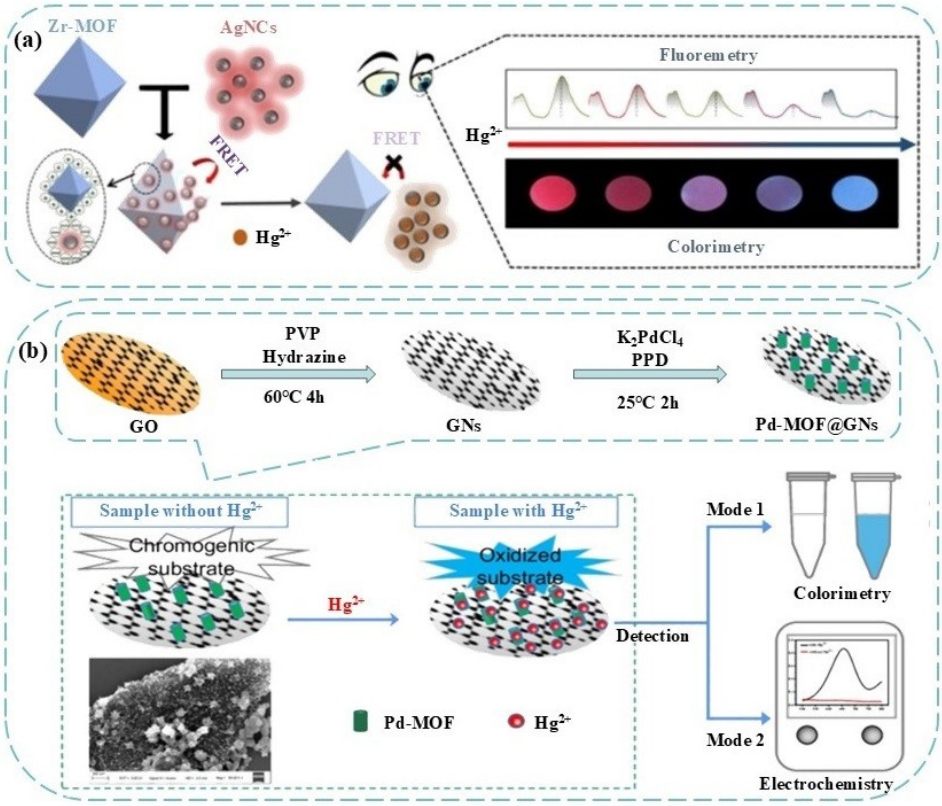

Figure 5. Dual-signal MOF sensors for Hg^{2+} detection: (a) Fluorescence and colorimetric signals and (b) colorimetric and electrochemical signals (revised from Liu et al.[18a] and Li et al.[18b]).

Microfluidic devices offer advanced approaches for manipulating and processing fluids on a microscale, with the potential for micron-level precision. They have numerous advantages, including low reagent consumption, enhanced efficiency, integration capabilities, and high levels of automation. This technology has found extensive applications in the detection of heavy metal pollutants, pesticide residues, small molecular compounds, pathogens, and microorganisms.[100] For example, Tatsuhiro et al.[101] integrated cell lysis microchannels, bioluminescence assay channels, micropumps, photometers, heaters, and temperature sensors into a transparent microfluidic device, utilizing these as the core components to develop an analyser for the measurement of adenosine triphosphate (ATP) in deep-sea environments. Measurements of ATP at various depths in the deep ocean yielded results consistent with those obtained through manual methods. This demonstrated that the ATP analyser developed was simple, accurate, and reliable in flow analysis and was suitable for real-time ATP assessment under extreme conditions. Furthermore, microfluidic technology can also be employed in the detection of heavy metals. For instance, Zhao et al.[102] developed a microchip-based lead sensor, which was subsequently moulded onto a glass substrate and crafted into a microdevice for the detection of lead in water, as depicted in Figure 6(a). The impact of interfering cations was assessed using a microfluidic device capable of detecting lead at concentrations as low as 5 parts per billion (ppb).

In paper microfluidics, filter paper or specialized paper is employed as the substrate to facilitate fluid transport via capillary action. In 2007, Whitesides et al.[103] developed a paper-based microfluidic device (μPAD) as a novel detection platform for qualitative and quantitative chemical analysis that was straightforward to operate and affordable. This device has a multi-layer microfluidic network, which facilitates both colorimetric and fluorescence detection. It has been widely applied in the identification of hazardous substances in various fields, including in medical diagnostics, water quality assessment, food safety, soil analysis, and plant studies.[104] For example, Zhang et al.[105] engineered antibiotics capable of simultaneously identifying Hg^{2+}, Ag^{+}, and aminoglycosides. This was achieved by integrating fluorescent-tagged functional single-stranded DNA with a graphene oxide sensor within a paper microfluidic device. As depicted in Figure 6(e), the paper microfluidic device was partitioned into two distinct zones, each dedicated to specific targets: the upper gray zone was designated for the detection of Hg^{2+} and Ag^{+}, while the lower green zone was tailored for antibiotic detection. The remaining two zones served as negative controls. The fluorophore-labelled T-rich SSDNA was adsorbed onto the graphene oxide surface, forming an open fluorescence sensor. This sensor was strategically positioned in the central zone of the μPAD, from where the

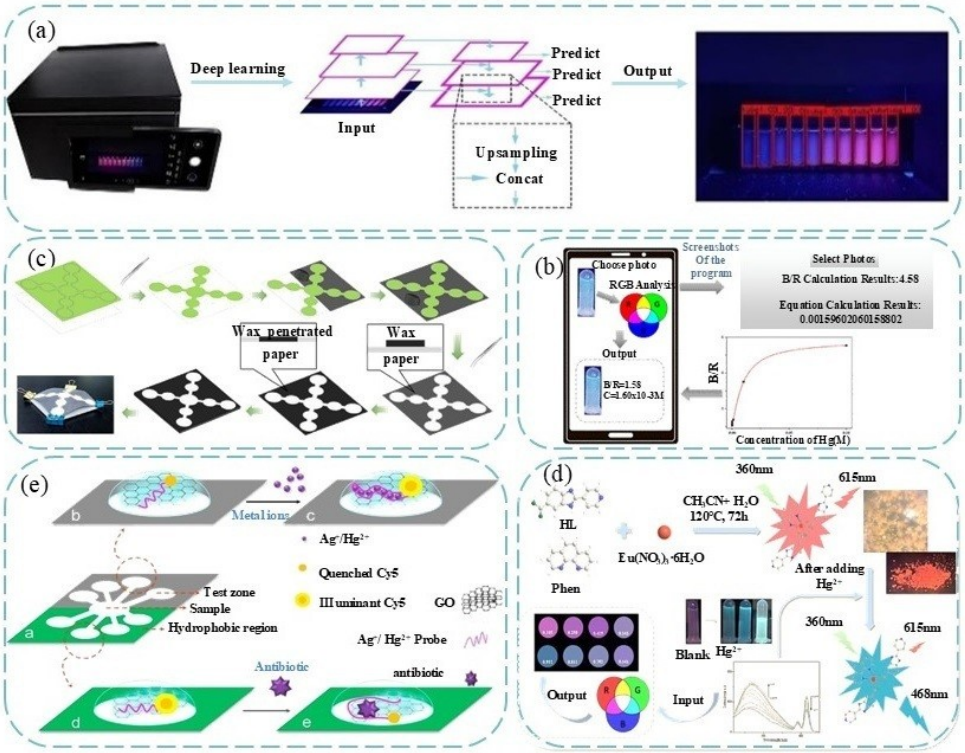

Figure 6. Integrated devices: (a) Microfluidics, (c) and (e) paper-based microfluidic devices, (b) and (d) mobile phones (according to Tang et al.,[58] Zhang et al.,[105] Zhu et al.,[65] Zhao et al.[102] and Yuan et al.[107]).

target-containing sample was drawn to the monitoring area via capillary action through a hydrophobic channel. In the presence of Hg^{2+}, the sensor in the detection area interacted with Hg^{2+}, resulting in the formation of a stable T-Hg^{2+}-T structure. Consequently, the T-rich SSDNA was set free from the graphene oxide surface, and the fluorescence signal was re-established. In 2019, Wu et al.[61] utilized AuNC/MIL-68(In)-NH_2/Cys hybrid materials as sensors along with the μPAD and developed a portable integrated device for detecting Hg^{2+} in real-world settings. The μPAD was engineered in the form of a radial star, featuring 12 detection reservoirs. This paper-based sensor was employed to detect Hg^{2+} in both lake and tap water, achieving a detection time of under 10 seconds. The μPAD demonstrated a distinct colour change, with a detection range spanning from 5.0 nM to 50 μM and a detection limit of 6.7 pM. The μPAD analysis device showed excellent selectivity and sensitivity, positioning it as a cost-effective, rapid detection platform.

In addition to microfluidic and paper-based devices, smartphones serve as portable tools for monitoring the detection process by capturing the photoelectric signals of target substances. These signals are then quantified using an app or external miniaturized devices.[106] Tang et al.[58] developed a smartphone-integrated sensor that utilized a hybrid of MOFs and quantum dots (QDs) for the visual detection of Hg^{2+}. Upon exposure to Hg^{2+}, the fluorescence of CdTe-QDs shifted from green to blue, whereas the fluorescence of NH_2-MIL-101(Fe) remained constant. Interestingly, the fluorescence of CdTe-QDs was observed to gradually revert to its original state upon the introduction of L-penicillamine (L-PA). As depicted in Figure 6(b), a fluorescent probe was integrated with a mobile application that captured the solvent's fluorescent colour under UV light. The application then translated the colour change into RGB values, enabling rapid detection of Hg^{2+} through the analysis of the ratio of green to blue channels. For real sample analysis, the sensor exhibited a linear response range of 0.12 to 1222 nM, with a detection limit of 0.091 nM for Hg^{2+}. Similarly, Zhu et al.[65] developed a mobile phone-based portable sensor for Hg^{2+} detection, which integrated the sensing method proposed by Tang et al. with Eu-MOFs, as depicted in Figure 6(d). This sensor was utilized for the detection of Hg^{2+} in tap water, lake water, and seawater, and recovery rates between 98.10% and 103.0% for Hg^{2+} were achieved. As an intelligent detection device, smartphone portable sensors offer advantages such as minimal requirements and swift data processing.

Furthermore, the integration of portable, paper-based devices with mobile phones for the detection of Hg^{2+} has been documented. For instance, Yuan et al.[107] engineered a multi-channel paper-based chip by creating hydrophobic and hydrophilic zones on filter paper. The hydrophilic zone comprised a buffer loading area, a detection zone, and a waste zone, as depicted in Figure 6(c). The fabricated paper-based chips were affixed to a black hydrophobic plate to prevent solution leakage and minimize the fluorescent background of the paper discs. During the detection of Hg^{2+}, the sample was introduced into the detection area of the multi-channel paper-based chip and positioned inside a dark box. The T-rich aptamer then bound

with Hg^{2+} to filter out the emissive material. Subsequently, Image J software was utilized on a smartphone to analyse the red, green, and blue (RGB) primary colour values in the image, facilitating the detection of varying concentrations of heavy metals in fruits and vegetables. The outcomes of the integrated device correlated well with those of ICP-MS detection, and the detection limit for Hg^{2+} was determined to be 1.7 nM.

Microfluidic, paper-based, and mobile phone portable sensors are pivotal elements of contemporary sensing technology, each with a unique set of advantages and drawbacks. Microfluidic sensors, which integrate multiple functions onto microchips, have low sample requirements and allow for rapid analysis, automation, and precise liquid manipulation and analysis. However, they may necessitate more complex maintenance and cleaning procedures. Paper-based sensors, on the other hand, are constructed from degradable materials that generate minimal environmental pollution and are convenient to carry without the need for complex equipment. Nevertheless, their detection ranges and sensitivity are constrained, and environmental factors can impact their performance and longevity. Smartphone portable sensors offer user-friendliness, robust data processing capabilities, widespread adoption potential, and the ability for remote communication. However, the absence of standardized protocols and calibration methods can lead to variable results across different devices, affecting the reproducibility of detection outcomes. In summary, portable devices offer a rapid, convenient, and efficient strategy for Hg^{2+} detection, enhancing user mobility, efficiency, and productivity. They are poised to facilitate the shift from laboratory to field-based Hg^{2+} detection.

4. Conclusions, Challenges and Perspectives

We summarize the progress on the development of MOF-based sensors for Hg^{2+} detection. The current MOFs used for Hg^{2+} detection consist mainly of MIL, UIO and ZIF MOFs. The recognition elements for Hg^{2+} include functional groups in the central ions and organic ligands of MOFs, T-rich aptamers, and surface-modified MNCs. Polymers of intrinsic microporosity and MOFs are known for their ability to incorporate functional groups such as amino, thiol, hydroxyl, sulfhydryl, and carboxyl groups within their organic ligands. Nonetheless, certain MOFs lack specific recognition sites, necessitating modification with T-rich DNA aptamers, for example, guanine and thymine-rich oligonucleotides tagged with carbon dots. These aptamers can form m-shaped DNA complexes through hybridization with complementary strands, thus creating a stable T-Hg^{2+}-T structure with Hg^{2+}. This method is commonly employed for Hg^{2+} recognition. However, due to the complexity of sample matrices and the significant effects of environmental factors, including pH, temperature, and the coexistence of other heavy metals, further enhancement in the specificity of Hg^{2+} identification is needed in sensors.

The detection signals are primarily optical, electrochemical, and photoelectrochemical dual-mode signals, along with auxiliary signals from portable devices. Optical and electrochemical signal detection has been utilized extensively for Hg^{2+} detection due to its high sensitivity, low detection limits, and simple instrumentation systems. Optical sensors are particularly convenient for on-site rapid detection, while electrochemical sensors offer high sensitivity and selectivity. In contrast, photoelectrochemical dual-mode sensors reduce background signals and improve accuracy. Moreover, portable devices can aid in Hg^{2+} detection while reducing costs and enabling on-site detection. This facilitates the identification and assessment of Hg contamination, providing timely warning of risks. The development of these sensors demonstrates that MOFs are promising in the of Hg^{2+} detection.

Although MOF sensors exhibit outstanding performance, several challenges must be overcome across a broad spectrum of applications. The current synthesis processes, structures, and properties of MOFs, along with the challenges associated with MOF sensors in Hg^{2+} detection applications, can be distilled into the following points. (1) Although numerous types of MOFs have been employed in Hg^{2+} detection, some MOFs have issues such as poor synthesis repeatability, complex synthesis processes, and low rates of reuse. (2) Although many types of MOFs have been utilized in Hg^{2+} detection and sensing technologies, the majority remain confined to laboratory exploration. Even when MOF samples are available, their use is typically limited to the laboratory verification stage, and they have not yet been deployed for large-scale on-site environmental testing. (3) With the strict requirements for environmental governance and food safety, it is imperative to further reduce the response times of Hg^{2+} detection sensors, streamline operational procedures, and enhance selectivity and sensitivity to ensure precise and rapid detection. (4) The stability of MOFs in actual Hg^{2+} detection environments and whether the concentration of central metal ions surpasses the bio-compatibility threshold for toxic effects remain unclear.

To promote the application of MOF-based sensors in detecting Hg^{2+}, future efforts should focus on refining the synthesis process of MOFs to optimize their structures and improve their efficiency and detection stability. By investigating the synergistic interactions between Hg and other heavy metals, the precision of Hg^{2+} detection could also be refined. The goal is to enable large-scale sensor production and establish a precise and rapid Hg^{2+} detection technique. These advances will not only facilitate highly sensitive detection of Hg^{2+} in real-world settings but also offer experimental and technical support for the development of portable devices, thereby enabling this Hg^{2+} detection technology to transition from the laboratory to field applications and providing a novel research approach for evaluating environmental and food-related Hg contamination.

Acknowledgements

The authors acknowledge the National Key Research and Development Program of China (2020YFC1807300), the National Natural Science Foundation of China (42377456, 22366014), Guizhou Provincial Science and Technology Projects (Guizhou

Provincial Major Scientific and Technological Program ([2024]013),Hubei Provincial Key Laboratory Open Fund for Selenium Resource Research and Biological Application (PT10202303, PT10202308, PT10202404), and Qiankehe Platform Talents-GCC [2023] 046), and the Youth Innovation Promotion Association CAS (2023415).

Conflict of Interests

The authors declare no conflict of interest.

Data Availability Statement

The data that support the findings of this study are available from the corresponding author upon reasonable request.

Keywords: Mercury (Hg) · Metal-organic framework (MOF) · Sensor · On-site detection · Portable devices

[1] a) J. Zhu, T. Wang, R. Talbot, H. Mao, X. Yang, C. Fu, J. Sun, B. Zhuang, S. Li, Y. Han, M. Xie, *Atmos. Chem. Phys.* **2014**, *14*, 2233–2244; b) C. T. Driscoll, R. P. Mason, H. M. Chan, D. J. Jacob, N. Pirrone, *Environ. Sci. Technol.* **2013**, *47*, 4967–4983; c) M. Chen, Y. Kong, W. Zheng, J. Liu, Y. Wang, Y. Wang, *Environ. Geochem. Health* **2024**, *46*, 83; d) A. Elwaleed, H. Jeong, A. H. Abdelbagi, N. T. Quynh, T. Agusa, Y. Ishibashi, K. Arizono, *Toxics* **2024**, *12*, 112; e) Z. Zhao, J. Yang, M. Zhao, J. Zhu, *J. Mater. Cycles Waste Manage.* **2023**, *25*, 2584–2598; f) M. Thiombane, B. De Vivo, B. Niane, M. J. Watts, A. L. Marriott, M. Di Bonito, *Environ. Geochem. Health* **2023**, *45*, 5067–5091; g) N. Basu, A. Bastiansz, J. G. Dórea, M. Fujimura, M. Horvat, E. Shroff, P. Weihe, I. Zastenskaya, *Ambio* **2023**, *52*, 877–896; h) G. M. Moulatlet, N. Yacelga, A. Rico, A. Mora, R. A. Hauser-Davis, M. Cabrera, M. V. Capparelli, *Chemosphere* **2023**, *339*, 139700.

[2] G. Qiu, X. Feng, S. Wang, L. Shang, *Environ. Pollut.* **2006**, *142*, 549–558.

[3] M. Horvat, V. Jereb, V. Fajon, M. Logar, J.-C. Bonzongo, J. Faganeli, M. Hines, *Geochem. Explor. Environ. Anal.* **2001**, *48*, 65–78.

[4] J. J. B. Nevadoa, L. F. G. Bermejoa, R. C. R. Martın-Doimeadios, *Environ. Pollut.* **2003**, *122*, 261–271.

[5] a) A. J. Ghoshdastidar, P. A. J. S. R. Ariya, *Sci. Rep.* **2019**, *9*, 10733; b) R. Harari, F. Harari, L. Gerhardsson, T. Lundh, S. Skerfving, U. Strömberg, K. J. T. I. Broberg, *Toxicol. Lett.* **2012**, *213*, 75–82; c) D. A. Rizzetti, F. Fernandez, S. Moreno, J. A. U. Ocio, F. M. Pecanha, G. Vera, D. V. Vassallo, M. M. Castro, G. A. Wiggers, *Brain Res.* **2016**, *1646*, 482–489.

[6] a) A. N. Alabssawy, A. H. Hashem, *Arch. Microbiol.* **2024**, *206*, 103; b) A. Mallongi, A. Rauf, R. Astuti, S. Palutturi, H. Ishak, *Global J. Environ. Sci. Manage.* **2023**, *9*, 261–274; c) L. Mao, W. Ren, X. Liu, M. He, B.-T. Zhang, C. Lin, W. Ouyang, *J. Hazardous Mater.* **2023**, *446*, 130724.

[7] A. Maulana, M. Harianti, T. B. Prasetyo, *J. Degraded Min. Lands Manage.* **2023**, *10*, 4791–4799.

[8] A. Witczak, M. Rajkowska-Myśliwiec, K. Pokorska-Niewiada, C. B. Navarro, *Food Chem. Toxicol.* **2024**, *191*, 114905.

[9] a) A. J. Ghoshdastidar, P. A. Ariya, *Sci. Rep.* **2019**, *9*, 10733; b) R. Harari, F. Harari, L. Gerhardsson, T. Lundh, S. Skerfving, U. Strömberg, K. Broberg, *Toxicol. Lett.* **2012**, *213*, 75–82; c) D. A. Rizzetti, F. Fernandez, S. Moreno, J. A. U. Ocio, F. M. Pecanha, G. Vera, D. V. Vassallo, M. M. Castro, G. A. J. B. r. Wiggers, *Brain Res.* **2016**, *1646*, 482–489.

[10] a) A. D. Singh, K. Khanna, J. Kour, S. Dhiman, T. Bhardwaj, K. Devi, N. Sharma, P. Kumar, N. Kapoor, P. Sharma, *Chemosphere* **2023**, *319*, 137917; b) N. Kumar, *Mercury Toxicity Mitigation: Sustainable Nexus Approach*, Springer **2024**, https://doi.org/10.1007/978-3-031-48817-7; c) D. C. King, M. J. Watts, E. M. Hamilton, R. Mortimer, D. P. Kilgour, M. Di Bonito, *Environ. Sci., Proc. Impacts* **2023**, *25*, 351–363; d) A. Joy, A. Qureshi, *Ambio* **2023**, *52*, 242–252.

[11] H. I. Qudus, P. Purwadi, I. Holilah, S. Hadi, *Molecules* **2021**, *26*, 3130.

[12] a) Y. Lei, F. Zhang, P. Guan, P. Guo, G. Wang, *New J. Chem.* **2020**, *44*, 14299–14305; b) D. Kozaki, M. Mori, S. Hamasaki, T. Doi, S. Tanihata, A. Yamamoto, T. Takahashi, K. Sakamoto, S. Funado, *Anal. Methods* **2021**, *13*, 1106–1109; c) K. E. Kristian, S. Friedbauer, D. Kabashi, K. M. Ferencz, J. C. Barajas, K. O'Brien, *J. Chem. Ed.* **2014**, *92*, 698–702.

[13] Y. Li, C. Chen, B. Li, J. Sun, J. Wang, Y. Gao, Y. Zhao, Z. Chai, *J. Anal. At. Spectrom.* **2006**, *21*, 94–96.

[14] a) J. R. Miranda-Andrades, S. Khan, M. J. Pedrozo-Penäfiel, B. A. Kátia de Cassia, R. M. Maciel, R. Escalfoni Jr, M. L. B. Tristao, R. Q. Aucelio, *Spectrochim. Acta Part B: At. Spectrosc.* **2019**, *158*, 105641; b) Y. Zhang, M. Miró, S. D. Kolev, *Talanta* **2018**, *178*, 622–628; c) L. R. Bravo-Sanchez, J. R. Encinar, J. I. F. Martınez, A. Sanz-Medel, *Spectrochim. Acta Part B: At. Spectrosc.* **2004**, *59*, 59–66.

[15] a) A. Thongsaw, R. Sananmuang, Y. Udnan, R. J. Ampiah-Bonney, W. C. Chaiyasith, *Anal. Sci.* **2019**, *35*, 1195–1202; b) H. Zheng, J. Hong, X. Luo, S. Li, M. Wang, B. Yang, M. Wang, *Microchem. J.* **2019**, *145*, 806–812; c) B. Zhao, M. He, B. Chen, B. Hu, *Spectrochim. Acta Part B: At. Spectrosc.* **2022**, *196*, 106524; d) T. Narukawa, T. Iwai, K. Chiba, *Talanta* **2020**, *210*, 120646

[16] a) S. Mukherjee, S. Bhattacharyya, K. Ghosh, S. Pal, A. Halder, M. Naseri, M. Mohammadniaei, S. Sarkar, A. Ghosh, Y. Sun, *Trends Food Sci. Technol.* **2021**, *109*, 674–689; b) A. Zuliani, N. Khiar, C. Carrillo-Carrión, *Anal. Bioanal. Chem.* **2023**, *415*, 2005–2023.

[17] D. Grieshaber, R. MacKenzie, J. Vörös, E. Reimhult, *Sensors* **2008**, *8*, 1400–1458.

[18] a) Z. Liu, R. Niu, M. Li, Z. Li, Y. Guo, *Microchim. Acta* **2024**, *191*, 352; b) W. Li, X. Zhang, X. Hu, Y. Shi, W. Xin, N. Liang, T. Shen, J. Xiao, M. Daglia, X. Zou, *Anal. Chim. Acta* **2022**, *1226*, 340153; c) L. Zhang, X. Bi, H. Wang, L. Li, T. You, *Talanta* **2024**, *273*, 125843.

[19] a) S. Liu, C. Lai, X. Liu, B. Li, C. Zhang, L. Qin, D. Huang, H. Yi, M. Zhang, L. Li, *Coord. Chem. Rev.* **2020**, *424*, 213520; b) R. Xu, Y. Cheng, X. Li, Z. Zhang, M. Zhu, X. Qi, L. Chen, L. Han, *Anal. Chim. Acta* **2022**, *1209*, 339893; c) A. A. Oladipo, S. D. Oskouei, M. Gazi, *Beilstein J. Nanotechnol.* **2023**, *14*, 631–673.

[20] M. A. Darwish, W. Abd-Elaziem, A. Elsheikh, A. A. Zayed, *Nanoscale Adv.* **2024**, *6*, 4015–4046.

[21] S. S. Shafqat, M. Rizwan, M. Batool, S. R. Shafqat, G. Mustafa, T. Rasheed, M. N. Zafar, *Chemosphere* **2023**, *318*, 137920.

[22] E. F. Hasan Alzaimoor, E. Khan, *Crit. Rev. Anal. Chem.* **2023**, *54*, 1–22.

[23] a) A. Khezerlou, M. Tavassoli, B. Khalilzadeh, A. Ehsani, H. Kazemian, *Food Control* **2023**, 109965; b) H. Kaur, N. Devi, S. S. Siwal, W. F. Alsanie, M. K. Thakur, V. K. Thakur, *ACS Omega* **2023**, *8*, 9004–9030; c) H. Sohrabi, S. Ghasemzadeh, Z. Ghoreishi, M. R. Majidi, Y. Yoon, N. Dizge, A. Khataee, *Mater. Chem. Phys.* **2023**, *299*, 127512; d) B. Mohan, A. Kamboj, K. Singh, G. Singh, A. J. Pombeiro, P. Ren, *Sep. Purif. Technol.* **2023**, *310*, 123175; e) Y. Jin, H. Liu, M. Feng, Q. Ma, B. Wang, *Adv. Funct. Mater.* **2024**, *34*, 2304773; f) K.-G. Liu, F. Bigdeli, Z. Sharifzadeh, S. Gholizadeh, A. Morsali, *J. Clean. Prod.* **2023**, *404*, 136709.

[24] a) W. Wu, Y. Li, P. Song, Q. Xu, N. Long, P. Li, L. Zhou, B. Fu, J. Wang, W. Kong, *Trends Food Sci. Technol.* **2023**, *138*, 238–271; b) M. Alizadeh Sani, G. Jahed-Khaniki, A. Ehsani, N. Shariatifar, M. H. Dehghani, M. Hashemi, H. Hosseini, M. Abdollahi, S. Hassani, Z. Bayrami, *Biosensors* **2023**, *13*, 94; c) B. Mohan, G. Singh, A. Chauhan, A. J. Pombeiro, P. J. J. o. H. M. Ren, *J. Hazardous Mater.* **2023**, *453*, 131324.

[25] a) B. Mohan, G. Singh, A. J. Pombeiro, A. A. Solovev, P. K. Sharma, Q. Chen, *TrAC Trends Anal. Chem.* **2023**, *159*, 116921; b) X. Lu, K. Jayakumar, Y. Wen, A. Hojjati-Najafabadi, X. Duan, J. Xu, *Microchim. Acta* **2024**, *191*, 58.

[26] a) P. S. Thakur, M. Sankar, *Mater. Lett.* **2022**, *311*, 131540; b) A. Wang, M. Walden, R. Ettlinger, F. Kiessling, J. J. Gassensmith, T. Lammers, S. Wuttke, Q. Peña, *Adv. Funct. Mater.* **2024**, *34*, 2308589; c) N. T. T. Nguyen, T. T. T. Nguyen, D. T. C. Nguyen, T. Van Tran, *Sci. Total Environ.* **2024**, *906*, 167295; d) S. Ghosh, A. Rana, S. Biswas, *Chem. Mater.* **2023**, *36*, 99–131; e) I. Abánades Lázaro, X. Chen, M. Ding, A. Eskandari, D. Fairen-Jimenez, M. Giménez-Marqués, R. Gref, W. Lin, T. Luo, R. S. Forgan, *Nat. Rev. Methods Primers* **2024**, *4*, 42.

[27] a) K. Manna, P. Ji, Z. Lin, F. X. Greene, A. Urban, N. C. Thacker, W. Lin, *Nat. Commun.* **2016**, *7*, 1–11; b) K. G. Pavithra, P. SundarRajan, P. S. Kumar, G. Rangasamy, *Chemosphere* **2023**, *312*, 137314; c) S. A. Younis, N. Bhardwaj, S. K. Bhardwaj, K.-H. Kim, A. Deep, *Coord. Chem. Rev.* **2021**, *429*, 213620.

[28] J. Yang, W. Zhu, W. Qu, Z. Yang, J. Wang, M. Zhang, H. Li, *Environ. Sci. Technol.* **2019**, *53*, 2260–2268.

[29] A. Soni, R. Sharma, D. S. Rana, D. Singh, N. Gupta, *Coord. Chem. Rev.* **2023**, *494*, 215343.

[30] a) P. Huang, W. Wu, M. Li, Z. Li, L. Pan, T. Ahamad, S. M. Alshehri, Y. Bando, Y. Yamauchi, X. J. C. C. R. Xu, *Coord. Chem. Rev.* **2024**, *501*, 215534; b) X. H. Liang, A.-X. Yu, X.-J. Bo, D.-Y. Du, Z.-M. J. C. C. R. Su, *Coord. Chem. Rev.* **2023**, *497*, 215427; c) B. Mohan, R. Kadiyan, K. Singh, G. Singh, K. Kumar, H. K. Sharma, A. J. J. M. J. Pombeiro, *Microchem. J.* **2023**, *190*, 108585; d) B. Mohan, S. Kumar, V. Kumar, T. Jiao, H. K. Sharma, Q. J. T. T. i. A. C. Chen, *TrAC Trends Anal. Chem.* **2022**, *157*, 116735; e) B. Mohan, G. Singh, A. Chauhan, A. J. Pombeiro, P. J. J. o. H. M. Ren, *J. Hazardous Mater.* **2023**, *453*, 131324; f) D. Manoj, S. Rajendran, T. K. Hoang, M. J. C. Soto-Moscoso, *Chemosphere* **2022**, *300*, 134516; g) D. Manoj, S. Rajendran, M. Murphy, A. Jalil, C. J. C. Sonne, *Chemosphere* **2023**, *340*, 139820.
[31] D. Dai, J. Yang, Y. Wang, Y. W. Yang, *Adv. Funct. Mater.* **2021**, *31*, 2006168.
[32] a) N. Garg, A. Deep, A. L. Sharma, *Crit. Rev. Anal. Chem.* **2024**, *54*, 1121–1145; b) S. S. A. Shah, M. Sohail, G. Murtza, A. Waseem, A. ur Rehman, I. Hussain, M. S. Bashir, S. S. Alarfaji, A. M. Hassan, M. A. Nazir, *Chemosphere* **2023**, *349*, 140729.
[33] M. U. Shahid, T. Najam, M. Islam, A. M. Hassan, M. A. Assiri, A. Rauf, A. ur Rehman, S. S. A. Shah, M. A. Nazir, *J. Water Process Eng.* **2024**, *57*, 104676.
[34] a) B. Mohanty, S. Kumari, P. Yadav, P. Kanoo, A. Chakraborty, *Coord. Chem. Rev.* **2024**, *519*, 216102; b) Q. Zhang, S. Yan, X. Yan, Y. Lv, *Sci. Total Environ.* **2023**, *902*, 165944; c) K. Boukayouht, L. Bazzi, S. El Hankari, *Coord. Chem. Rev.* **2023**, *478*, 214986; d) G. Lin, B. Zeng, J. Li, Z. Wang, S. Wang, T. Hu, L. Zhang, *Chem. Eng. J.* **2023**, *460*, 141710.
[35] C. Jia, T. He, G.-M. J. C. C. R. Wang, *Coord. Chem. Rev.* **2023**, *476*, 214930.
[36] P.-L. Wang, L.-H. Xie, E. A. Joseph, J.-R. Li, X.-O. Su, H.-C. J. C. Zhou, *Chem. Rev.* **2019**, *119*, 10638–10690.
[37] Z. Mo, H. Zhang, A. Shahab, J. Chen, C. Huang, *J. Taiwan Inst. Chem. Eng.* **2023**, *146*, 104778.
[38] S. Ghosh, F. Steinke, A. Rana, S. Biswas, *Inorg. Chem. Front.* **2022**, *9*, 859–869.
[39] S. Wang, Y. Wang, J. Ma, C. Huang, L. Chen, *Anal. Bioanal.Chem.* **2024**, *416*, 1001–1010.
[40] Y.-F. Zhang, Z.-H. Zhang, H. Fang, X.-A. Guo, Y.-N. Ma, Y.-Z. Zhang, D.-X. Xue, *Inorg. Chem.* **2023**, *62*, 20513–20519.
[41] W. Li, X. Zhang, X. Hu, Y. Shi, W. Xin, N. Liang, T. Shen, J. Xiao, M. Daglia, X. J. A. C. A. Zou, *Anal. Chim. Acta* **2022**, *1226*, 340153.
[42] Z. Wang, Z. Lv, A. Guo, G. Hu, J. Liu, J. Huang, *Sensors and Actuators Reports* **2022**, *4*, 100120.
[43] P. Zhang, H. Cheng, F. Gu, S. Hong, H. Dong, C. Li, *Surf. Interfaces* **2023**, *42*, 103368.
[44] a) J. Xu, Y. Zhang, X. Zhu, G. Ling, P. Zhang, *J. Hazardous Mater.* **2024**, *465*, 133424; b) O. Ozalp, Z. P. Gumus, M. Soylak, *J. Mol. Liquids* **2023**, *378*, 121589.
[45] M. Krüger, A. K. Inge, H. Reinsch, Y.-H. Li, M. Wahiduzzaman, C.-H. Lin, S.-L. Wang, G. Maurin, N. Stock, *Inorg. Chem.* **2017**, *56*, 5851–5862.
[46] K. Tang, Y. Chen, S. Tang, X. Wu, P. Zhao, J. Fu, H. Lei, Z. Yang, Z. J. S. T. T. E. Zhang, *Sci. Total Environ.* **2023**, *856*, 159073.
[47] H. Xiao, W. Zhang, Q. Yao, L. Huang, L. Chen, B. Boury, Z. Chen, *Appl. Catal., B* **2019**, *244*, 719–731.
[48] J. Jiang, Y. Lu, J. Liu, Y. Zhou, D. Zhao, C. Li, *J. Solid State Chem.* **2020**, *283*, 121153.
[49] K. M. Ismail, S. S. Hassan, S. S. Medany, M. A. Hefnawy, *Mater. Adv.* **2024**, *5*, 5870–5884.
[50] M. Guo, J. Chi, Y. Li, G. I. Waterhouse, S. Ai, J. Hou, X. Li, *Microchim. Acta* **2020**, *187*, 1–8.
[51] R.-L. Yu, Q.-F. Li, Z.-L. Li, X.-Y. Wang, L.-Z. Xia, *ACS Appl. Mater. Interfaces* **2023**, *15*, 35082–35091.
[52] M. Tu, D. E. Kravchenko, B. Xia, V. Rubio-Giménez, N. Wauteraerts, R. Verbeke, I. F. Vankelecom, T. Stassin, W. Egger, M. Dickmann, *Angew. Chem. Int. Ed.* **2021**, *60*, 7553–7558.
[53] a) J. Dalmieda, P. Kruse, *Sensors* **2019**, *19*, 5134; b) M. Loya, S. Ghosh, A. K. Atta, *J. Mol. Struct.* **2023**, *1278*, 134949.
[54] a) S. C. Hung, C.-C. Lu, L.-C. Chen, *IEEE Sensors J.* **2021**, *21*, 23949–23956; b) M. Dhanushkodi, G. G. V. Kumar, B. K. Balachandar, S. Sarveswari, S. Gandhi, J. Rajesh, *Dyes Pigments* **2020**, *173*, 107897; c) G. A. Bodkhe, D. D. Khandagale, M. S. More, M. A. Deshmukh, N. N. Ingle, P. W. Sayyad, M. M. Mahadik, S. M. Shirsat, M. Al-Buriahi, M.-L. Tsai, *Ceram. Int.* **2023**, *49*, 6772–6779.
[55] S.-Q. Liu, J.-S. Chen, X.-P. Liu, C.-J. Mao, B.-K. Jin, *Analyst* **2023**, *148*, 772–779.
[56] J. Cui, X. Xu, C. Yang, J. Wang, Q. Guo, G. Nie, *Sens. Actuators, B* **2023**, *378*, 133141.
[57] S. Ghosh, F. Steinke, A. Rana, S. J. I. C. F. Biswas, *Inorg. Chem. Front.* **2022**, *9*, 859–869.
[58] K. Tang, Y. Chen, S. Tang, X. Wu, P. Zhao, J. Fu, H. Lei, Z. Yang, Z. Zhang, *Sci. Total Environ.* **2023**, *856*, 159073.
[59] T. Xia, T. Song, G. Zhang, Y. Cui, Y. Yang, Z. Wang, G. Qian, *Chem.–A Eur. J.* **2016**, *22*, 18429–18434.
[60] A. Pankajakshan, D. Kuznetsov, S. Mandal, *Inorg. Chem.* **2019**, *58*, 1377–1381.
[61] X.-J. Wu, F. Kong, C.-Q. Zhao, S.-N. Ding, *Analyst* **2019**, *144*, 2523–2530.
[62] X. Wang, Z. Jiang, C. Yang, S. Zhen, C. Huang, Y. Li, *J. Hazard. Mater.* **2022**, *423*, 126978.
[63] Z. Lu, J. Li, K. Ruan, M. Sun, S. Zhang, T. Liu, J. Yin, X. Wang, H. Chen, Y. Wang, *Chem. Eng. J.* **2022**, *435*, 134979.
[64] R. Zhang, J. Yang, Y. Cao, Q. Zhang, C. Xie, W. Xiong, X. Luo, Y. He, *Spectrochim. Acta, Part A* **2024**, *312*, 124062.
[65] J. Zhu, L. Fan, W. Li, X. Qi, C. Sun, W. Li, Z. Chang, *J. Photochem. Photobiol., A* **2024**, *452*, 115583.
[66] X. Wang, H. Wang, L. Guo, G. Chen, R. Kong, F. Qu, L. Xia, *Analyst* **2020**, *145*, 1362–1367.
[67] A. Radwan, I. M. El-Sewify, A. Shahat, H. M. Azzazy, M. M. Khalil, M. F. El-Shahat, *ACS Sustainable Chem. Eng.* **2020**, *8*, 15097–15107.
[68] Q. Song, L. Wang, J. Zhang, Y. Liu, X. Zhang, X. Kong, *Spectrochim. Acta, Part A* **2024**, *312*, 124013.
[69] Y. Zhang, J. Song, Q. Pan, X. Zhang, W. Shao, X. Zhang, C. Quan, J. Li, *J. Mater. Chem. B* **2020**, *8*, 114–124.
[70] S. Singh, A. Numan, Y. Zhan, V. Singh, T. Van Hung, N. D. Nam, *J. Hazard. Mater.* **2020**, *399*, 123042.
[71] X. Wang, M. Xu, Y. Kuang, X. Liu, J. Yuan, *J. Hazard. Mater.* **2024**, *465*, 133169.
[72] H. Yang, C. Peng, J. Han, Y. Song, L. Wang, *Sens. Actuators, B* **2020**, *320*, 128447.
[73] X. Zhang, M. Zhu, Y. Jiang, X. Wang, Z. Guo, J. Shi, X. Zou, E. Han, *J. Hazard. Mater.* **2020**, *400*, 123222.
[74] K. Doloi, N. Badhai, D. Mohanta, *Mater. Res. Bull.* **2024**, *170*, 112558.
[75] D. Luo, J. Huang, Y. Jian, A. Singh, A. Kumar, J. Liu, Y. Pan, Q. J. J. M. C. B. Ouyang, *J. Mater. Chem. B* **2023**, *11*, 6802–6822.
[76] a) X. Yan, H. Ge, *Int. J. Biol. Macromol.* **2023**, *232*, 123329; b) L. Geng, J. Huang, M. Fang, H. Wang, J. Liu, G. Wang, M. Hu, J. Sun, Y. Guo, X. Sun, *Food Chem.* **2024**, *458*, 140330.
[77] B. ElTaher, R. Sabouni, M. Ghommem, A. Alami, *Int. J. Environ. Sci. Technol.* **2022**, *19*, 12193–12210.
[78] S. S. Patil, V. N. Narwade, K. S. Sontakke, T. Hianik, M. D. Shirsat, *Sensors* **2024**, *24*, 346.
[79] A. Ono, H. Togashi, *Angew. Chem. Int. Ed.* **2004**, *116*, 4400–4402.
[80] C. Liu, Y. Wang, Y. Li, S. Meng, W. Li, D. Liu, T. You, *Sci. Total Environ.* **2023**, *900*, 166407.
[81] a) H. Nabipour, S. Rohani, S. Batool, A. S. Yusuff, *J. Environ. Chem. Eng.* **2023**, *11*, 109131; b) F. Hassani, A. Larki, M. Ghomi, N. Pourreza, *Spectrochim. Acta Part A: Mol. Biomol. Spectrosc.* **2023**, *302*, 123104; c) J. Kaur, M. Kaur, S. K. Kansal, A. Umar, H. Algadi, *Chemosphere* **2023**, *311*, 136832.
[82] J. Dong, L. Wen, D. Zhao, H. Yang, J. Zhao, Z. Hu, Y. Ma, C. Hou, D. Huo, *Food Chem.* **2023**, *418*, 135869.
[83] a) S. Menon, S. P. Usha, H. Manoharan, P. V. N. Kishore, V. Sai, *ACS Sensors* **2023**, *8*, 684–693; b) Q. Y. Yang, C.-Q. Wan, Y.-X. Wang, X.-F. Shen, Y.-H. Pang, *J. Hazardous Mater.* **2023**, *451*, 131148.
[84] a) J. Milikić, M. Savić, A. Janošević Ležaić, B. Šljukić, G. Ćirić-Marjanović, *Polymers* **2024**, *16*, 683; b) S. A. A. Razavi, A. Morsali, *Coord. Chem. Rev.* **2020**, *415*, 213299; c) H. Singh, A. Bamrah, S. K. Bhardwaj, A. Deep, M. Khatri, K.-H. Kim, N. Bhardwaj, *J. Hazardous Mater.* **2021**, *407*, 124379; d) B. Mohan, R. Kadiyan, K. Singh, G. Singh, K. Kumar, H. K. Sharma, A. J. Pombeiro, *Microchem. J.* **2023**, *190*, 108585.
[85] a) M. R. Han, W.-X. Dong, S.-S. Feng, L.-P. Lu, Z.-P. Li, *Dalton Trans.* **2021**, *50*, 4944–4951; b) J. Chen, H. Chen, T. Wang, J. Li, J. Wang, X. Lu, *Anal. Chem.* **2019**, *91*, 4331–4336.
[86] a) C. Liang, S. Tan, L. Shao, X. Xue, J. Liu, N. Liu, W. Zhang, Q. Shi, *Inorg. Chem.* **2023**, *62*, 9508–9517; b) X. Lin, F. Luo, L. Zheng, G. Gao, Y. Chi, *Anal. Chem.* **2015**, *87*, 4864–4870; c) J. Zhao, Y.-N. Wang, W.-W. Dong, Y.-P. Wu, D.-S. Li, Q.-C. Zhang, *Inorg. Chem.* **2016**, *55*, 3265–3271.
[87] a) Z. Chen, J. Ma, D. W. Sun, *Compr. Rev. Food Sci. Food Saf.* **2023**, *22*, 2977–3010; b) B. Jie, H. Lin, Y. Zhai, J. Ye, D. Zhang, Y. Xie, X. Zhang, Y. Yang, *Chem. Eng. J.* **2023**, *454*, 139931.
[88] A. S. Holmes-Smith, *Biosens. Bioelectron.* **2015**, *5*, 616–617.

[89] A. H. Alshatteri, G. K. Ali, K. M. Omer, *ACS Appl. Mater. Interfaces* **2023**, *15*, 21239–21251.
[90] Z. Ali, R. Ullah, M. Tuzen, S. Ullah, A. Rahim, T. A. Saleh, *Trends Environ. Anal. Chem.* **2023**, *37*, e00187.
[91] X. Zou, L. Huang, Y. Liu, Q. Chen, X. Zheng, M. Fan, Z. Gong, *Sens. Actuators, B* **2023**, *393*, 134121.
[92] H. Sohrabi, F. Maleki, P. Khaaki, M. Kadhom, N. Kudaibergenov, A. Khataee, *Biosensors (Basel)* **2023**, *13*, 347.
[93] Z. Chen, C. Zhang, Q. Gao, G. Wang, L. Tan, Q. Liao, *Anal. Chem.* **2015**, *87*, 10963–10968.
[94] B. Mohan, R. Kumari, G. Singh, K. Singh, A. J. Pombeiro, X. Yang, P. Ren, *Environ. Int.* **2023**, *175*, 107928.
[95] X. Fu, B. Ding, D. D'Alessandro, *Coord. Chem. Rev.* **2023**, *475*, 214814.
[96] a) G. Wang, J. Liu, F. Yue, Z. Shen, D. Xu, H. Fang, W. Chen, Z. Wang, P. Li, Y. J. L. Guo, *LWT* **2022**, *165*, 113658; b) Q. Huang, F. Luo, C. Lin, J. Wang, B. Qiu, Z. Lin, *Biosens. Bioelectron.* **2021**, *189*, 113374; c) J. Liu, L. Geng, H. Wang, J. Huang, G. Wang, Z. Shen, M. Hu, B. Li, J. Sun, J. Dong, *Sensors Actuators B: Chem.* **2024**, *410*, 135665.
[97] A. Sharma, A. Singh, V. Gupta, A. K. Sundramoorthy, S. Arya, *Trends Environ. Anal. Chem.* **2023**, *38*, e00200.
[98] S. Sonwal, V. K. Gupta, S. Shukla, R. Umapathi, S. M. Ghoreishian, S. Han, V. K. Bajpai, Y. Cho, Y. S. Huh, *Adv. Colloid Interface Sci.* **2024**, *331*, 103199.
[99] a) M. Yuan, C. Li, Y. Zheng, H. Cao, T. Ye, X. Wu, L. Hao, F. Yin, J. Yu, F. Xu, *Talanta* **2024**, *266*, 125112; b) P. Kamnoet, W. Aeungmaitrepirom, R. F. Menger, C. S. Henry, *Analyst* **2021**, *146*, 2229–2239; c) F. Li, Y. Hu, Z. Li, J. Liu, L. Guo, J. He, *Anal. Bioanal. Chem.* **2019**, *411*, 6497–6508; d) K. Kant, M.-A. Shahbazi, V. P. Dave, T. A. Ngo, V. A. Chidambara, L. Q. Than, D. D. Bang, A. Wolff, *Biotechnol. Adv.* **2018**, *36*, 1003–1024.
[100] a) R. Umapathi, S. M. Ghoreishian, S. Sonwal, G. M. Rani, Y. S. Huh, *Coord. Chem. Rev.* **2022**, *453*, 214305; b) J. H. Lin, S.-J. Chen, J.-E. Lee, W.-Y. Chu, C.-J. Yu, C.-C. Chang, C.-F. Chen, *Chem. Eng. J.* **2022**, *430*, 133070.
[101] T. Fukuba, T. Noguchi, K. Okamura, T. Fujii, *Micromachines (Basel)* **2018**, *9*, 370.
[102] L. Zhao, T. Wu, J.-P. Lefèvre, I. Leray, J. A. Delaire, *Lab Chip* **2009**, *9*, 2818–2823.
[103] A. W. Martinez, S. T. Phillips, M. J. Butte, G. M. Whitesides, *Angew. Chem. Int. Ed.* **2007**, *119*, 1340–1342.
[104] H. Liu, R. M. Crooks, *J. Am. Chem. Soc.* **2011**, *133*, 17564–17566.
[105] Y. Zhang, P. Zuo, B.-C. Ye, *Biosens. Bioelectron.* **2015**, *68*, 14–19.
[106] W. Xiao, M. Xiao, Q. Fu, S. Yu, H. Shen, H. Bian, Y. Tang, *Sensors* **2016**, *16*, 1871.
[107] M. Yuan, C. Li, Y. Zheng, H. Cao, T. Ye, X. Wu, L. Hao, F. Yin, J. Yu, F. J. T. Xu, *Talanta* **2024**, *266*, 125112.

Manuscript received: October 11, 2024
Accepted manuscript online: November 20, 2024
Version of record online: December 4, 2024